Published in final edited form as:

*FASEB J.* 2021 June ; 35(6): e21615. doi:10.1096/fj.202002610R.

# Exomer complex regulates protein traffic at the TGN through differential interactions with cargos and clathrin adaptor complexes

**Carlos Anton-Plagaro**[1,2,*], **Noelia Sanchez**[1], **Rosario Valle**[1], **Jose Miguel Mulet**[3], **Mara C. Duncan**[4], **Cesar Roncero**[1,*]

[1]Instituto de Biología Funcional y Genómica (IBFG) and Departamento de Microbiología y Genética, CSIC-Universidad de Salamanca, Salamanca, Spain

[2]Present address: School of Biochemistry, University of Bristol, Bristol, UK

[3]Instituto de Biología Molecular y Celular de Plantas, CSIC-Universitat Politècnica de València, Valencia, Spain

[4]Cell and Developmental Biology Department, University of Michigan, Ann Arbor, MI, USA

## Abstract

Protein sorting at the *trans* Golgi network (TGN) usually requires the assistance of cargo adaptors. However, it remains to be examined how the same complex can mediate both the export and retention of different proteins or how sorting complexes interact among themselves. In *Saccharomyces cerevisiae*, the exomer complex is involved in the polarized transport of some proteins from the TGN to the plasma membrane (PM). Intriguingly, exomer and its cargos also show a sort of functional relationship with TGN clathrin adaptors that is still unsolved. Here, using a wide range of techniques, including time-lapse and BIFC microscopy, we describe new molecular implications of the exomer complex in protein sorting and address its different layers of functional interaction with clathrin adaptor complexes. Exomer mutants show impaired amino acid uptake because it facilitates not only the polarized delivery of amino acid permeases to the PM but also participates in their endosomal traffic. We propose a model for exomer where it modulates the recruitment of TGN clathrin adaptors directly or indirectly through Arf1 function. Moreover, we describe an *in vivo* competitive relationship between the exomer and AP-1 complexes for the model cargo Chs3. These results highlight a broad role for exomer in regulating protein sorting at the TGN that is complementary to its role as cargo adaptor and present a model to understand the complexity of TGN protein sorting.

[*]Corresponding authors: - Dr. Carlos Anton-Plagaro, Biomedical Sciences Building (University of Bristol), Tankard's Cl, University Walk, Bristol BS8 1TD, UK, carlos.antonplagaro@bristol.ac.uk; - Prof. Cesar Roncero, IBFG, C/ Zacarías González, 37007, Salamanca, Spain, crm@usal.es, Phone: 34-923-294883 FAX: 34-923-224876.

AUTHOR CONTRIBUTIONS

CR and CAP designed the research and CAP performed most of the experiments. NS, RV, JMM and MCD did experimental work and/or provided essential reagents. CR and CAP wrote the paper and generated the figures. MCD contributed to the final text editing. All authors have read and approved the final manuscript.

CONFLICT OF INTEREST STATMENT

The authors state explicitly there are no conflicts of interest in connection with this article.

## INTRODUCTION

The trans Golgi network (TGN) is a major intracellular cargo sorting station, where newly synthesized proteins and endocytosed proteins need to be accurately identified and sorted to distinct subcellular destinations (1). Cells utilize sophisticated cargo sorting machineries to meticulously package the cargo molecules into the right transport carriers (1). During this process, cargo adaptors often play pivotal roles in both cargo recognition and in coat assembly (2, 3), while coat assembly ultimately leads to membrane deformation and fission (4). One critical coat at the TGN is the clathrin coat, which generates clathrin-coated vesicles (CCV). Although it is clear that in most eukaryotes the clathrin adaptor complex-1 (AP-1) plays a critical role in TGN sorting, growing evidence suggests it may play a role in both export and retention, moreover AP-1 shows genetic interaction with several other sorting complexes suggesting communication between complexes may help maintain the protein sorting function (2, 3). CCV assembly has been extensively analyzed in the yeast *Saccharomyces cerevisiae* (5). In this yeast, several clathrin adaptors are sequentially recruited to TGN membranes through a coordinated mechanism that depends on PtdIns(4)P and the Arf1 GTPase (3). The adaptor complex GGA is first recruited, followed by AP-1. Deletion of Gga2 alters the dynamics of the recruitment of AP-1. By contrast, AP-1 has minor mechanistic effects in the assembly of the other clathrin adaptor complexes (6). Clathrin and its adaptor complexes have a general role in the regulation of the traffic of multiple proteins to the pre-vacuolar compartment (PVC) facilitating their recycling back to the TGN. Accordingly, the involvement of these complexes in the late endosomal traffic of multiple amino acid transporters has been described (7–10). Recycling from the PVC has been well characterized for TGN resident proteins like Kex2, Vps10 and Tlg1 (11–13). However, a role for clathrin in the formation of a distinct subset of secretory vesicles has also been reported (14), but the nature of these vesicles and their cargos has remained elusive.

The function of clathrin and its adaptors in the anterograde traffic from the TGN to PM is poorly understood, yet another sorting complex, exomer, has a more established role in this TGN to PM traffic. The exomer complex is a cargo adaptor required for the delivery of three cargoes to the PM, the major chitin synthase, Chs3, (15–17), Fus1 (18), and Pin2 (19), all three integral transmembrane proteins. Exomer consists of a tetramer formed by a dimer of the scaffold protein Chs5 and two accessory proteins (20) that are encoded by four different genes: the paralogous *BCH1* / *BUD7* and *CHS6* / *BCH2* gene pairs (17, 21). Together these four proteins are called the ChAPs (Chs5-Arf1 binding proteins). The ChAPs are thought to bind directly to cargos, Arf1, and membranes thereby acting as the cargo recognition face of the complex. The current view is that any two of the four ChAPs can be incorporated into the exomer complexes, providing different functionalities (21–23). For example, only an exomer containing the Chs6 ChAP is able to mediate the traffic of Chs3 to the PM (17, 21, 24), because Chs3 interacts physically with the exomer through the Chs6 ChAP (24–26). In contrast, the Bch1 Bud7 paralogous proteins appear to interact directly with the TGN membrane to favor the membrane curvature required for vesicle formation (22).

Interestingly, all known exomer cargos are also subject to AP-1-mediated traffic (18, 19, 27). This was first reported for Chs3, where deletion of the AP-1 complex restores Chs3 PM

localization in cells lacking exomer (25, 27). This restoration is thought to indicate a role for clathrin and AP-1 in the retention of Chs3 at the TGN (27), which allows the exomer to deliver Chs3 to the PM in a cell cycle or stress-regulated manner (28). The mechanistic relationship between exomer and AP-1 complexes in this retention mechanism is unclear. In addition, exomer is well conserved in other fungi (21, 29), and it has been recently reported that the *Schizosaccharomyces pombe* exomer interacts functionally with clathrin adaptors as a means to maintain the integrity of diverse cellular compartments (30). Taken together, these results, reported in several organisms, highlight the potential multiple levels of interaction among exomer and other TGN complexes in order to facilitate protein traffic.

In this work, we explored additional roles for exomer in protein traffic and its unsolved relationship with TGN clathrin adaptors using multiple aproaches. We show that exomer not only facilitates the anterograde traffic of several integral PM proteins from the TGN, but also plays a general role in protein traffic by modulating the assembly of TGN clathrin adaptors thus regulating proper traffic from the TGN to the PVC. Finally, we conclude that exomer maintains different associations with cargos and clathrin adaptors, which differ along fungal lineage.

## MATERIAL AND METHODS

### Yeast strains construction.

The yeasts strains used throughout this work were made in the W303, BY4741 or X2180 genetic backgrounds as indicated in the Table 1. Cells were transformed using lithium acetate/ polyethylene glycol procedure (31). Gene deletions were made using a PCR-mediated gene replacement technique, using different deletion cassettes based on the *natMX4*, *kanMX4*, or *hphNT1* resistance genes (32). For the insertion of the GAL1 promoter in front of ORFs, the cassette was amplified from pFA6a-*kanMX4*::pGAL1 (33) (Table 2). Proteins were tagged chromosomally at their C-terminus with 3xHA, GFP, mCherry and Venus CT or NT fragments, employing integrative cassettes amplified from pFA6a-*3xHA::hphMx6*/ pFA6a-*GFP::hphMx6*/ pFA6a-*GFP::natMx4*/ pFN21/ pFA6a-*VN::HIS3Mx6*/ pFA6a-*VC::kanMX6* (34). The *Delitto Perfetto* technique was performed to generate the internal gene modifications within the genome. In brief, this approach allows for *in vivo* mutagenesis using two rounds of homologous recombination. The first step involves the insertion of a cassette containing two markers at or near the locus to be altered and the second involves complete removal of the cassette and transfer of the expected genetic modification to the chosen DNA locus as previously described (35).

*Construction of TAT2$^{52\text{-}53}$-3xHA*. To obtain a fully functional tagged version of Tat2, we generated a chromosomally internally-tagged version of Tat2 in a region suitable for causing less reduced interference in Tat2 function, regulation and transport (between amino acids 52-53) using the *Delitto Perfetto* technique. Contrary to the GFP versions, this HA tagged protein fully complemented the *tat2Δ*-associated phenotypes, and importantly, had no effect on the *chs5Δ* requirement for external tryptophan. For microscopic localization we used a GFP C-terminus tagged version of the protein. This protein is functional based on the complementation of the *tat2Δ* mutant, but showed a reduced rate of endocytosis (36).

The *C. albicans* mutants were generated as previously described (29).

## Media and growth assays.

Yeast cells were grown at 28ºC in YEPD (1 % Bacto yeast extract, 2 % peptone, 2 % glucose), in SD medium (2 % glucose, 0.7 % Difco yeast nitrogen base without amino acids) or SD-N (2 % glucose, 0.16 % Difco yeast nitrogen base without ammonium and amino acids) supplemented with the pertinent amino acids and 2 % agar in the case of solid media. Calcofluor white (CW) sensitivity was always tested on YEPD or SD medium buffered with 50 mM potassium phthalate at pH 6.2 as described (37).

**C. albicans media.—**LEE (2 % agar, 0.5 % $(NH_4)_2SO_4$, 0.25 % $K_2HPO_4$, 0.02 % $MgSO_4 \cdot 7H_2O$, 0.5 % NaCl, 0.05 % proline, 1.25 % glucose), LEE NAGA (LEE w/o glucose + 1.25 % N-Acetylglucosamine), LEE SERUM (LEE + 4 % fetal bovine serum) and M199 (M199 [Gibco BRL], 2 % agar, 80 mg/L uridine).

**Drop tests.—**To assess the growth phenotypes, cells of each tested strain from early logarithmic cultures were resuspended in water and adjusted to an $OD_{600}$ of 1.0. Ten-fold serial dilutions were prepared and drops were spotted onto the appropriate agar plates containing media supplemented as indicated. Plates were incubated at 28ºC for 2–5 days.

**Quantification of half maximal inhibitory concentration (IC50).—**Sensitivity to myriocin and sertraline was analyzed in liquid YEPD media by growing strains in a 96-well plate with different drug concentrations and measuring the $OD_{600}$ using a Spectra Max 340PC plate reader as described in (38).

## Fluorescence microscopy.

Yeast cells expressing GFP/ mCherry/ Venus tagged proteins were grown to early logarithmic phase in SD medium supplemented with 0.2 % adenine. Living cells were visualized directly by fluorescence microscopy. The bimolecular fluorescence complementation (BIFC) technique was used to analyze proximity among different proteins *in vivo* (39). For CW staining, 50 μg/ml CW was directly added to the fresh cells growing in YEPD and the cultures were incubated at 28ºC for 1h before images were taken (40).

For non-quantitative purposes, images were routinely obtained using a Nikon 90i Epifluorescence microscope (x100 objective; NA: 1.45) equipped with a Hamamatsu ORCA ER digital camera, specific Chroma filters (49000 ET-DAPI, 49002 ET-GFP, 49003 ET-YFP, 49005 ET-DsRed) and controlled by *Metamorph* software. Images for quantitative purposes, such as co-localization, particle description or stream time-lapse of TGN-tagged proteins were acquired in a Spinning Disk confocal microscope (Olympus IX81 with Roper technology) with an Evolve EMCCD camera, 100X/1.40 Plan Apo lens, 488nm / 561nm lasers, 525/45 – 609/54 Semrock emission filters and controlled by *Metamorph* 7.7 software.

## Protein extracts and immunoblotting.

The trichloroacetic acid (TCA) protocol was used for protein processing for the Western blot analyses. Extracts were made using an equal numbers of cells from logarithmic growing

cultures. Cells were centrifuged, resuspended in 20 % TCA, and frozen at −80ºC for at least 3 hours. The samples were then thawed on ice and the centrifuged cells were disrupted in 1.5 ml tubes with 100 µl of 20 % TCA and glass beads (0.45 mm, SIGMA), during 3 pulses of 30 seconds with an intensity of 5.5 in a Fast prep (FP120, BIO101). Extracts were transferred to new tubes and 5% TCA was added to dilute TCA concentration to 10 %. Precipitated proteins were collected by centrifugation at 900xg for 10 min and the supernatant was completely discarded. Pelleted proteins were resuspended in 50 µl of 2x Sample Buffer (100 mM Tris-HCl pH 6.8, 4 % SDS, 20 % glycerol, 25 mM DTT and traces of bromophenol blue) by vortexing, followed by the addition of 50µl of 2 M Tris-HCl pH 7.5. Samples were maintained on ice throughout this process. Finally, the extracts were heated to 37ºC for 30 min (for multipass transmembrane proteins) or 95ºC for 5 min (for other proteins) and centrifuged for 5 min at 15000xg. The supernatant was collected and 15µl were used for Western blot analysis.

Extracts were separated on 7.5 % SDS-PAGE and transferred to PVDF membranes (37). The membranes were then blocked with TBST (Tris-buffered saline with 0.1% Tween 20) supplemented with 3 % non-fat dry milk for 1 hour and incubated with the corresponding antibodies in TBST with 3 % milk for 2 h at room temperature (RT) or overnight (O/N) at 4ºC: anti-GFP JL-8 monoclonal antibody (Living colors, Clontech), anti-HA 12CA5 (Roche), anti-tubulin (T5162 Sigma). The blots were developed using anti-Rsp6-P (Cell SignalingTech: Phospho-Ser/Thr Akt Substrate Antibody #9611s) and 5 % BSA replaced the non-fat dry milk in all steps. After 3 washes with TBST, the membranes were incubated for 50 min together with the secondary antibodies in TBST with 3 % milk: polyclonal anti-Mouse or anti-Rabbit conjugated with horseradish peroxidase. After 3 washes with TBST, the blots were developed using the ECL kit (Advansta).

### Subcellular fractionation by centrifugation in a sucrose gradient.

For subcellular fractionations, 50 ml of culture with an $OD_{600}$ of 0.8–1 were collected and $NaN_3$ and NaF were added up to a final concentration of 20 mM. The cultures were centrifuged at 4ºC at 4000xrpm for 4 min, resuspended with ice-cold water in 1.5 ml tubes, centrifuged at 6000xrpm for 2 min and resuspended in 1 ml of Azida Buffer (10 mM DTT, 20 mM $NaN_3$, 20 mM NaF, 100 mM Tris-HCl pH 9.4). After a 10-minute incubation step at RT, the samples were centrifuged at 6000xrpm for 2 min and resuspended in 600 µl of Spheroplast Buffer (1 M sorbitol, 20 mM $NaN_3$, 20 mM NaF, 10 mM Tris-HCl pH 7.5 in YEPD medium). Afterwards, 60 µl of zymolyase (100T, unfiltered, 4.76 mg/ml) were added and incubated at 30ºC during 30–40 min under gentle mixing until spheroplasts were produced based on microscopic analysis. The spheroplast samples were then washed twice with spheroplast buffer and collected by 500xg centrifugation for 4 min at 4ºC. The washed spheroplasts were incubated with 300 µl Lysis Buffer (10 % sucrose, protease inhibitors, 1 mM PMSF, 1 mM EDTA, 20 mM Tris-HCl pH 7.5) and incubated 10 min at RT with gradual pipetting (6-8 times). Lysis was microscopically assessed. Then, cell debris was removed by centrifugation at 500xg for 4min at 4ºC, the supernatants were collected and 250 µl of the supernatants were layered on the top of a mini-step sucrose gradient (EDTA 5 mM, 50 mM Tris-HCl pH7.5) made as follows: 300 µl 55%, 750 µl 45%, 500 µl 41%, 300 µl 37%, 250 µl 29%. The gradients were centrifuged at 200,000xg for 3.5 h at 4ºC (Beckman

Coulter L-80 XP, SW 55 Ti rotor) and 7 fractions of 300 µl were manually collected from the top of the gradient. Finally, 100 µl of each fraction were denatured in the sample buffer plus 1 % SDS for 30 min at 37ºC.

### Tryptophan uptake assay.

Tryptophan was measured adapting protocols previously described (36, 41). Specifically, cells were grown to early log phase in 50 mL of SD medium (without Trp) at 30°C until an $OD_{600}$ of 0.4–0.8. Then, the cells were washed twice with wash buffer (10 mM sodium citrate, pH 4.5, and 20 mM $(NH_4)_2SO_4$) and resuspended in 3.6 ml of incubation medium (10 mM sodium citrate, pH 4.5, 20 mM $(NH_4)_2SO_4$, and 2 % glucose). The absorbance at 600 nm was measured to refer values to cell number. The assay was initiated by the addition of 400 µl of radiolabeled tryptophan solution (390 µl of the incubation medium and 10 µl of L-[5-$^3$H]-tryptophan at 31 Ci/mmol GE healthcare, UK). Two aliquots (500 µl) were collected at each time point and chilled by the addition of 1 ml of the ice-cold incubation medium. Cells were collected by filtration through a nitrocellulose filter (0.45 µm pore size, 25 mm diameter [Millipore HAWP]) and washed three times with chilled water. Moist filters were transferred to Filter Count solution (Perkin Elmer, USA). Radioactivity was measured using a Tri-Carb® 4910 TR liquid scintillation counter (Perkin Elmer, USA).

### Digital quantification, statistics and figure design.

Microscopy and Western blot image processing and quantification were performed using *ImageJ-FIJI* software (1.48k version, NIH). For quantification of dot co-localization, pre-filtering with a custom built *ImageJ* Macro (Macro1, see Table 3) was used followed by the analysis of the co-localization using the JACoP *ImageJ* plugin (co-localization based on centers of mass-particles coincidence, particle size 4−∞ pixels). For the particle descriptors (intensity and area), ROIs were selected using a custom built Macro (Macro2, see Table 3), applying the same intensity threshold per-experiment and loaded to ROIManager with AnalyzeParticles (0.07−∞ µm$^2$, exclude on edges). In the case of Chs3-GFP TGN-EE structures, due to the difficulty of the segmentation, dots were selected manually for maximum intensity and maximum diameter quantification. A more detailed description of the macros used is presented in the supplementary materials.

For the quick time-lapse experiments, continuous images were acquired through the streaming mode on a Spinning Disk microscope in 3 z-planes separated by 0.2 µm to avoid loss of the highly dynamic TGN-structures in z-axis and to partially reduce photo-bleaching. Z-maximum intensity projections were analyzed manually or with the TrackMate *ImageJ* plugin. For the Sec7-mR2 structures, tracking was done using the TrackMate *ImageJ* plugin (LoG detector, Diameter 0.5 µm, Threshold 80, Median filter, Sub-pixel loc.; LAP Tracker; Frame to Frame 0.5 µm, No Gap, Split 0.5µM, Merge 0.5 µm, tracks with ≥ 5 spots). The analysis was performed only on tracks that initiated and completed during the collection. For analyzing the recruitment of the exomer and clathrin adaptor complexes, images were taken of strains expressing *CHS5*-mCh/*GGA1*-GFP and *CHS5*-mCh/*APS1*-GFP. Afterwards, only the trajectories of structures showing both signals (mCh/GFP), present for ≥10 s, were selected manually or with the help of TrackMate (LoG detector, Diameter 1 µm, Threshold 15–30, Median filter, Sub-pixel loc.; LAP Tracker; Frame to Frame 0.5 µm, No Gap,

No Split, No Merge, Duration ≥ 8s) and the *Extract track stack* option (half of vesicles extracted from each channels). The average recruitment duration (temporal region with intensity ≥ 25 % of the maximum intensity per channel), as well as the temporal distance between maximum intensity peaks referring to Chs5-mCh for 30 trajectories, were manually calculated.

To obtain an unbiased measurement of the cellular polarization of PM proteins, the daughter/mother plasma membrane signal coefficient (polarization coefficient) of single cells was determined as described (42).

Image measurements were statistically analyzed using the T-test for unpaired data in *GraphPad Prism* 6 software (GraphPad Software, Inc., La Jolla, USA). Significantly different values ($P < 0.05$, $P < 0.01$, $P < 0.001$, $P < 0.0001$) are indicated (*, **, ***, ****).

The presented images were prepared using *Adobe Photoshop CS5* and *Adobe Illustrator CS5* (San José, CA, USA) software. All images shown in each series were acquired under identical conditions and processed in parallel to preserve the relative intensities of fluorescence for comparative purposes. If not indicated, the scale bar represents 5 μm.

## RESULTS

### Exomer mutants show ammonium sensitivity due to the reduced uptake of tryptophan.

Exomer has been described to function as a cargo adaptor complex based on its role in the transport of Chs3, the catalytic subunit of the major chitin synthase in budding yeast (17, 21, 24). However, our recent work, based on the evolutionary characterization of exomer function across the fungi kingdom, suggests exomer may have additional functions (29). More importantly, *S. cerevisiae* exomer mutants showed multiple phenotypes that cannot be explained by known cargoes of exomer such as sensitivity to ammonium (21, 29).

In an effort to better understand the functionality of exomer, we first confirmed the ammonium sensitivity of the exomer mutant *chs5Δ* by showing that this mutant grew poorly in YEPD supplemented with 0.2 M ammonium (Figure 1A). This sensitivity was also observed in SD media (Figure S1A). Interestingly, the absence of the two paralogous pairs of ChAPs produced different growth phenotypes (Figure 1A). The *bch1Δ bud7Δ* double mutant was as sensitive to ammonium as *chs5Δ*; however *chs6Δ bch2Δ* double mutant was not sensitive to ammonium. This result is notable since Chs6/Bch2 are known to function as cargo adaptors, whereas Bch1/Bud7 are thought to function in membrane association without cargo selectivity (22–24). These results could therefore reflect a role for exomer that is independent of its function as cargo adaptor.

A first indication for the source of the ammonium sensitivity of the exomer mutants came from the observation that the *chs5Δ* mutant was not sensitive to ammonium in the prototrophic X2180 background (Figure S1A). Although ammonium toxicity in yeast is poorly understood, one mechanism for ammonium detoxification involves the active excretion of amino acids across the PM (43). We hypothesized that as cells excrete amino

acids as a response to ammonium toxicity, they deplete internal pools of amino acids and the prototrophic strain is able to compensate by synthesizing higher levels of the essential amino acids. We further pinpointed the key auxotrophic requirement through the observation that the *chs5Δ* mutant was not sensitive to ammonium in the BY strain, which differs from W303 in that it is not auxotrophic for tryptophan. In order to confirm this, we transformed the *chs5Δ* mutant in the W303 background with different plasmids that restore the ability to synthesize amino acids for each auxotrophy. The restoration of the ability to synthesize tryptophan by a plasmid encoding *TRP1*, strongly reduced the ammonium sensitivity of the *chs5Δ* mutant, while the plasmid containing *HIS3* and *URA3* genes showed no effect on ammonium sensitivity (Figure S1B). By contrast, restoration of the ability to synthesize leucine by a plasmid encoding *LEU2* slightly reduced ammonium sensitivity. Moreover, the addition of tryptophan to the medium also abolished ammonium sensitivity in all strains. These results could indicate that the *chs5Δ* mutant has a reduced uptake of tryptophan, and, therefore, this mutant may require higher amounts of external tryptophan for growth. Consistent with this model, the wild-type auxotroph strain in SD media could form colonies with as little as 0.001 mg/ml of tryptophan, while the *chs5Δ* mutant required 8 times more tryptophan in the medium to obtain substantial colony growth (Figure 1B). In order to confirm these results, we measured tryptophan uptake directly (Figure 1C). Consistent with the increased requirement for extracellular tryptophan, tryptophan uptake was severely reduced in the absence of exomer compared to wild-type yeast. However, uptake was not as low as cells lacking the tryptophan permease Tat2 (44). Together these results show that in exomer mutants, the deficient uptake of tryptophan restricts the growth of tryptophan auxotrophs in a low concentration of tryptophan or in the presence of ammonium.

## Deficient Trp uptake of exomer mutants is directly linked to Tat2 permease but independent on nitrogen source regulation.

In yeast, tryptophan is primarily transported by one of two permeases, the general amino acid permease, Gap1, and the high affinity specific Trp-permease, Tat2 (45). In media containing high ammonium levels, such as SD, Gap1 is not expressed; therefore, we hypothesized that the *chs5Δ* defect could be associated with defects in Tat2 localization or function. Consistent with this hypothesis, overexpression of *TAT2* suppressed the ammonium sensitivity of *chs5Δ* (Figure S1C). These results strongly suggest that ammonium and tryptophan phenotypes observed in *chs5Δ* are caused by defective function of Tat2 permease. Notably, the ammonium sensitivity of the double mutant *tat2Δ chs5Δ* was not fully suppressed by external tryptophan (Figure S1C, D), suggesting that the absence of exomer may affect additional amino acid transporters. This conclusion is consistent with the partial alleviation of ammonium sensitivity after *LEU2* introduction (Figure S1B). As an additional test of the effect of exomer on amino acid transporters, we analyzed the sensitivity of exomer mutants to toxic analogs of different amino acids (46–50). Sensitivity to these analogs can indicate changes in the plasma membrane levels or activity of the relevant amino acid transporter. In the X2180 background, the exomer mutant *chs5Δ* was moderately more sensitive to the arginine analogue Canavanine, but significantly more resistant to the proline analogue AzC, to the *HIS3* inhibitor 3-AT and to toxic concentrations of histidine (Figure 1D). These results are consistent with a potential defect in the uptake of

several amino acids, owing to a defect in the localization or function of several amino acid permeases (AAPs).

Alternatively, the observed phenotypes could simply reflect a defect in the regulation of nitrogen metabolism in the absence of exomer. To test this possibility, we first investigated whether the *chs5Δ* mutant showed altered signaling through the Ssy1p-Ptr3p-Ssy5 (SPS) sensor of extracellular amino acids (45) (Figure S2B). We first compared the phenotypes of the cells lacking SPS to those of cells lacking exomer. We found that the phenotype of *ssy1Δ*, the core SPS sensor, was not identical to that of *chs5Δ*. Unlike *chs5Δ*, *ssy1Δ* was resistant to canavanine and sensitive to 3-AT, although similar to *chs5Δ* it was resistant to AzC (Figure S2A). Moreover, *chs5Δ ssy1Δ* double mutant exhibited phenotypes of sensitivity to canavanine and resistance to AzC, 3-AT and to toxic concentrations of histidine as that of *chs5Δ*. We then monitored whether loss of exomer disrupted SPS function. We found that the localization of Ssy1-GFP in the *chs5Δ* strain was indistinguishable from the wild type (Figure S2C). More importantly, loss of exomer did not affect the proteolytic processing of the SPS effector Stp1 in response to amino acids, a key step in the SPS signaling pathway (45) (Figure 1E). Taken together, these observations indicate that the SPS signaling pathway is fully functional in the absence of exomer.

As an additional test for whether exomer controls amino acids signaling, we investigated the TORC1 pathway, which regulates many AAPs (45). TORC1 signaling occurs in preferred nitrogen sources like glutamine and during this signaling, two kinase regulatory subunits, Gtr1 and Tco89, are recruited to the vacuolar membrane, from where they triggers the phosphorylation of the small ribosomal subunit, Rsp6, and the Nitrogen Catabolite Repression (NCR) signaling pathway transcription factor, Gln3 (51, 52) (Figure S2D). We found that Gtr1 and Tco89 localized normally at the vacuolar membrane in the *chs5Δ* mutant (Figure S2E), the phosphorylation timing of Rps6 occurred normally in this mutant upon growth in different nitrogen sources (Figure 1F) and the levels of Gln3 phosphorylation were indistinguishable from control under different nutritional conditions (Figure S2F).

All of these results strongly indicate that nitrogen signaling occurs normally in the absence of exomer. We therefore hypothesized that the observed phenotypes might be associated directly with a defective transport of one or several AAPs.

### Exomer is required for proper intracellular traffic of the Tat2 and Mup1 permeases.

In order to test this hypothesis, we first monitored the localization of the amino acid permeases Tat2 and Mup1. These proteins localized at the PM in induction media under steady-state conditions (Figure 2A) in either the wild-type or *chs5Δ* mutant strains. However, in the *chs5Δ* mutant, Tat2 was conspicuously absent at the vacuole and some of the protein was localized in intracellular spots. Similarly, Mup1 was also localized in intracellular spots in the absence of exomer. Terminally-tagged versions of Tat2 show impaired endocytosis (see materials and methods section and references therein). Therefore, to confirm whether Tat2 localization changes in *chs5Δ*, we performed subcellular fractionations using an internally HA-tagged version of Tat2 (Figure 2B). In the wild-type strain, Tat2–3xHA localized primarily in the lightest fractions of the gradient together with Pma1, a marker of the plasma membrane fraction. However, in the *chs5Δ* mutant Tat2–

3xHA showed a bimodal distribution, with part of the protein co-migrating with Pma1 and the other significant part co-migrating with the TGN/endosomal marker Pep12 in the heavier fractions. These observations suggest that *chs5Δ* causes partial intracellular accumulation of Tat2 and Mup1 at the TGN/endosomal compartment. This event would lead to a reduction in the levels of the permeases at the PM, leading to the tryptophan and amino acid analog responses described above.

The steady state localization of AAPs reflects the balance of anterograde transport of newly synthesized proteins, endocytosis, and recycling. Therefore, the mislocalization of Tat2 or Mup1 could reflect a defect in any of these steps. To test whether exomer contributes to anterograde traffic of Tat2 and Mup1, we used a regulated expression system based on the GAL1 promoter. Growth on galactose induces expression thus allowing us to examine anterograde transport based on the arrival of each permease at the PM. One hour after induction, both proteins were readily apparent at the plasma membrane in both wild-type and *chs5Δ* cells, suggesting that the overall rate of anterograde traffic is not dramatically reduced in *chs5Δ* cells (Figure 2C). However, both Tat2 and Mup1 were less polarized in the *chs5Δ* mutant. In wild-type cells, both Tat2 and Mup1 were highly polarized in the growing bud, whereas in the *chs5Δ* mutant a significant amount of each transporter was observed spread along the PM of the mother cell. A quantitative analysis of Tat2 and Mup1 distribution indicated that the PM signal in the daughter cells is significantly reduced in the absence of the exomer for both proteins (Figure 2D). Although the functional significance of the defect in polarized distribution is unclear, these results indicate that exomer contributes to the polarized delivery of these proteins to the PM, in a similar fashion to what has been described for Ena1 (42).

Following on, we examined the effect of exomer on the behavior of AAPs after endocytosis. Tat2 is endocytosed after the depletion of tryptophan from the media and trafficked to the vacuole for degradation (53). In a wild-type strain, Tat2-GFP signal was increased in the vacuole after tryptophan depletion and the total amount of the protein was significantly reduced (Figure 2E). However, in the *chs5Δ* mutant, fluorescence in the vacuole was reduced compared to the wild type, and intracellular spots became more numerous and intense (Figure 2E). In addition, the total amount of Tat2 was significantly higher in the *chs5Δ* mutant than in the wild type after tryptophan depletion. Mup1 is also rapidly endocytosed, trafficked to the vacuole and degraded in presence of an excess of methionine in wild-type cells (Figure 2F) (54). Similar to Tat2, in cells lacking exomer Mup1 traffic to the vacuole was reduced 20 minutes after adding methionine, with fewer cells showing vacuolar fluorescence and more cells showing substantial plasma membrane signal in the *chs5Δ* mutant compared to the wild type. This defect was associated with an increase in the number of cells with bright intracellular spots. However, vacuolar localization was apparent in *chs5Δ* after 45 minutes. Analysis of the total levels of Mup1 by Western blot after adding methionine indicated that protein degradation was significantly delayed in the absence of exomer (Figure 2F). These results are consistent with a function for exomer in the proper traffic of AAPs, and may explain the phenotypes associated with *chs5Δ* in terms of the cells being sensitive to different levels of tryptophan and toxic amino acids.

### Exomer dependent recycling of Tat2 differs from that of Chs3.

Based on the proposed role of exomer in the recycling of Chs3 (27), we tested whether exomer controlled the recycling of Tat2. In yeast, the recycling of Tat2 and Mup1 depends on the f-box protein Rcy1 (55). To determine whether exomer contributes to this step in recycling, we first compared the phenotypes of *rcy1Δ* and *chs5Δ* mutants. We found that *rcy1Δ* was sensitive to ammonium, and, as previously reported, required an external supply of tryptophan for growth (55) (Figure 3A,B). These results are consistent with a model that proposes that both exomer and Rcy1 may participate in the recycling of AAPs. Interestingly, the double *rcy1Δ chs5Δ* mutant required a greater concentration of tryptophan for growth than the single-gene deletion mutants, which could suggest Rcy1 and exomer act at different steps in recycling or that the recycling pathway is only partially functional in the absence of either factor (Figure 3B).

To distinguish between these possibilities, we explored the genetic interactions between *chs5Δ* and *rcy1Δ* and additional regulators of Tat2. We first examined clathrin adaptors Gga1 and Gga2, which alter cell surface levels of Tat2 in some mutant backgrounds by controlling sorting from the TGN to the vacuole (36). We found that *chs5Δ* and *rcy1Δ* showed different effects when combined with deletion of *gga2Δ*, or the *gga1Δ gga2Δ* double mutant (Figure 3C). The ammonium sensitivity of *chs5Δ* was suppressed by *gga2Δ* and more so by the *gga1Δ gga2Δ* double mutation. In contrast, the *rcy1Δ* phenotype was not suppressed by *gga2Δ*. Interestingly, the *gga1Δ* mutant was sensitive to ammonium on its own, a sensitivity that was additive with the *chs5Δ* mutant, but not with the *rcy1Δ* mutant. Together these results suggest that exomer and Rcy1 may affect different steps of AAPs trafficking.

The suppression of the ammonium sensitivity of *chs5Δ* by *gga2Δ* is reminiscent of the previously reported suppression of the calcofluor resistance of *chs5Δ* by *gga2Δ* (27, 56). We therefore sought to determine whether the exomer-mediated traffic of Tat2 was similar to the exomer-mediated traffic of Chs3. In addition to Gga1 and Gga2, the clathrin adaptor protein complex AP-1 alters the traffic of Chs3 in exomer mutant cells (27). We first asked whether deletion of the small subunit of AP-1 (*aps1Δ*) suppressed the ammonium sensitivity of *chs5Δ.* Unlike calcofluor resistance, *aps1Δ* did not suppress the ammonium sensitivity of *chs5Δ* (Figure 3D). Similarly, *aps1Δ* did not suppress the sensitivity of *chs5Δ* to low tryptophan while *gga2Δ* did it efficiently (Figure S3), suggesting that the traffic of Chs3 and AAPs are strikingly different.

To further explore the differential requirements for Chs3 and AAP traffic, we explored the role of the arrestin family of ubiquitin ligase adaptors because the recycling of Tat2 is controlled by its ubiquitination mediated by the Bul1 arrestin-like protein (57). Accordingly, *bul1Δ* suppressed the ammonium sensitivity of the *chs5Δ* mutant (Figure 3A). In contrast, after analyzing calcofluor sensitivity and staining, the deletion of *BUL1* did not restore Chs3 PM transport in the *chs5Δ* mutant (Figure 3A, E). Because Bul1 is one of a number of arrestin-like adaptors, we also tested the partially redundant Bul2 ligase, the *bul1Δ bul2Δ* double mutant, and individual deletions of ten additional arrestin ligases. None of the arrestin mutants suppressed the calcofluor resistance of *chs5Δ*, highlighting the difference between AAPs and Chs3 (See Figure S4). In summary, while both Tat2 and Chs3 proteins can be re-routed by Gga2 proteins in the absence of exomer, the two proteins likely diverge

at one or more steps in their traffic, suggesting that the mechanistic requirement for exomer differs for the two proteins.

## Exomer is involved in traffic to late endosomes by modulating the proper assembly of the clathrin adaptor complexes.

Exomer and clathrin adaptors mediate the traffic of common cargoes including Chs3 and AAPs, however, their functions appear to be largely antagonistic to one another. Mechanistically, this antagonism could be explained by direct physical competition between exomer and clathrin adaptors for cargo, or something more complex. In order to understand the antagonistic roles of exomer and clathrin adaptors, we explored their proximity to one another using bi-molecular fluorescence complementation (BIFC) (39). Exomer comes into close proximity to both AP-1 and Gga2, based on the appearance of fluorescent puncta in strains containing Chs5-VN and either Apl4-VC or Gga2-VC. Our BIFC results also confirmed the previously reported physical interaction of exomer with its cargo Chs3 (Figure 4A), but also revealed close proximity of exomer with Mup1 (Figure 4A), suggesting exomer may play a direct role in Mup1 traffic.

Because BIFC can trap transient proximity between proteins and does not report on the dynamic changes in protein localization, we next addressed the dynamic TGN localization of exomer and clathrin adaptors using two-channel spinning disk-confocal microscopy (Figure 4B, Figure S5). Previous work has established an ordered recruitment of clathrin adaptors, with Gga2 reaching peak fluorescence several seconds before AP-1 (6, 58). We found that exomer is recruited shortly after GGA, and significantly before (21.9 seconds) AP-1 (Figure 4B), a temporal distribution that overlaps with both clathrin adaptor complexes. This distribution is also consistent with the co-localization observed between exomer and GGA and AP-1 complexes (Figure S5E).

Next, we explored whether the absence of exomer affected the localization of clathrin adaptors. In the *chs5Δ* mutant, Gga2 collapsed in significantly brighter and larger puncta compared to wild-type cells (Figure 4C,D) and similar results were observed for the AP-1 (Apl4) complex. Moreover, co-localization between Gga2 and Apl4 was significantly increased in the *chs5Δ* mutant compared with the control (Figure 4C,E).

In order to confirm the physiological relevance of these defects, we determined the sensitivity of the *chs5Δ* mutant to sertraline and myriocin. These drugs affect membrane fluidity and lipid biosynthesis, and selectively inhibit the growth of yeast with impaired AP-1 functions (59, 60). We found that *chs5Δ* mutant was significantly more sensitive to both drugs, showing a half maximal inhibitory concentration (IC50) of 0.087 ± 0.005 mM and 6.60 ± 0.33 mM to myrocin and sertraline respectively, IC50s significantly ($p<0.01$) lower than those observed for the wild-type strain (0.178 ± 0.011 mM and 8.16 ± 0.19 mM). This increased sensitivity to both drugs is consistent with altered AP-1 function in the *chs5Δ* mutant (Figure 4F).

## Re-exploring the functional link between Arf1 GTPase and the exomer complex.

Exomer was described as an Arf1 GTPase-dependent protein complex (13,15) and was later co-crystalized with Arf1 (14). Interestingly, TGN clathrin adaptors also bind Arf1 GTPase

(6, 20). Therefore, the antagonistic functions of these complexes may be through direct competition for active Arf1.

We next sought to monitor the effects of exomer on Arf1 localization. Unfortunately, GFP tagging of Arf1 disrupts its function (61) and alters TGN/EE morphology (Figure S6A), similarly to what has been described for the null mutant (62). We therefore analyzed as an alternative the localization of Sec7, a guanine nucleotide exchange factor (GEF) that stimulates Arf1 activity at the TGN (63) promoting clathrin adaptor localization (6). We found that similar to clathrin adaptors, the intensity and area of Sec7 puncta were greater in the *chs5Δ* mutant (Figure 5A). Moreover, time-lapse analysis showed that in the exomer mutant *chs5Δ* the Sec7 dots moved significantly slower and showed reduced track displacement, although the lifespan of the structures was only slightly increased (Figure 5B, Figure S6B,C). The functional significance of this altered movement is unclear but, altogether, our results suggest that exomer could influence the behavior of clathrin adaptors through Arf1/Sec7. In view of this implication of exomer in Arf1/Sec7 dynamics, we sought to revisit the role of Arf1/Sec7 in exomer functionality.

We first addressed the effect of the *arf1Δ* mutation. Surprisingly this mutant showed increased levels of chitin based on calcofluor staining (Figure 5C, upper panels), which were in clear agreement with increased levels of Chs3 at the bud neck (Figure 5C, lower panels, see arrows and amplified insets), despite the partial accumulation of part of this protein in aberrant TGN/EE structures (Figure 5C, lower panels, see arrowheads). The absence of Arf1 reversed the effect of the *chs5Δ* mutation on calcofluor staining and Chs3 localization as previously described (27), likely through rerouting Chs3 to the PM in a less polarized fashion (Figure 5C). Similar results were obtained when we depleted Arf1 by growing the *pGAL1-ARF1* strain in glucose. (Figure 5D, E). Moreover, Arf1 depletion in glucose also relieved the calcofluor and tryptophan phenotypes associated with the *chs5Δ* mutant (Figure 5D, E and S6D). Although the effects of Sec7 were difficult to assess due its absence being lethal, the transient depletion of Sec7 in the pGAL-*SEC7* strains after growth in glucose slightly increased chitin synthesis in the wild-type strain and restored chitin synthesis in the *chs5Δ* mutant (Figure 5D,E).

Interestingly, overexpression of either Arf1 or Sec7 in the wild-type strain after growth in galactose caused hypersensitivity to calcofluor (Figure 5D), which in the case of Sec7 could be linked to an increased deposition of chitin towards the bud (Figure 5E). However, the overexpression of either protein did not restore chitin synthesis in *chs5Δ*. In contrast, overexpression of Sec7, but not of Arf1, alleviated the tryptophan and ammonium phenotypes of *chs5Δ* mutant (Figure 5D and S6D), suggesting that Sec7 has a different effect on the traffic of amino acid permeases.

Finally, given the ability of exomer to influence the localization of clathrin adaptors, we tested the effect of GGA overexpression on exomer function using the GAL1 promoter. We found that the overexpression of Gga2 in a wild-type strain significantly reduced the recruitment of exomer and AP-1 complexes at the TGN (Figure S7A–D). However, this overexpression did not produce a significant physiological effect on chitin synthesis or ammonium sensitivity, probably because Gga2 exerts a pleiotropic effect on both complexes

(Figure S7E, F). Remarkably, in the absence of the exomer complex, overexpression of Gga2 partially recovered chitin synthesis and diminished sensitivity to ammonium (Figure S7E, F). While the chitin phenotype could be explained by alteration of the AP-1 complex, which in turn promotes the aperture of the alternative route for the chitin synthase to the PM, the ammonium phenotype is probably more complex and likely associated with general alterations of the TGN.

Altogether our results support the existence of a complex network of functional interactions between Arf1, exomer and clathrin adaptors. Moreover, although it is known that Arf1 activity favors the polarized delivery of Chs3 by exomer, this activity, contrary to previous reports (17), was found not to be essential for exomer function since polarization of Chs3 occurred normally in the absence of Arf1/Sec7 (Figure 5C), when exomer was still present at the TGN/EE membranes (Figure S6E). In contrast, the ablation of Arf1/Sec7 function reroutes Chs3 and amino acid permeases to the PM, independently of exomer, through alternative route/s likely to be associated with the effects of this ablation in the recruitment of clathrin adaptors (6). Interestingly, overexpression of Sec7 only had a significant effect on the traffic of amino acid permeases in the absence of exomer, reinforcing our previous findings (see above) that suggest that different links exits between exomer and Chs3 and amino acid permeases.

## The intracellular traffic of the exomer bona fide cargoes is dependent on their competitive interactions between exomer and AP-1 complexes.

Previous studies suggest that exomer assembled by different ChAPs subunits may have dramatically different functions. The Chs6/Bch2 pair is proposed to directly mediate association with selected cargoes like Chs3, whereas the Bch1/Bud7 pair contributes to exomer association with membranes and membrane remodeling together with Arf1 (22–24). Given the effects of exomer on clathrin adaptors, we revisited the roles of the different exomer subunits in the traffic of Chs3.

In the absence of a functional exomer (*chs5Δ*), or when both members of a group of ChAP paralogs are deleted *(chs6Δ bch2Δ* or *bch1Δ bud7Δ*), yeast cells become resistant to calcofluor owing to the intracellular retention of Chs3 (review in (64)). However, we found that in the complete absence of functional exomer the subcellular localization of Chs3 differed compared to the loss of the cargo binding paralogs Chs6/Bch2. In the absence of a functional exomer (*chs5Δ*), Chs3 was found in significantly brighter puncta compared to the wild type (Figure 6A), similar to what was observed for Gga2/Apl4 in this mutant (Figure 4C). A similar phenotype was also seen in the *bch1Δ bud7Δ* double mutant (Figure S8B). However, in the *chs6Δ bch2Δ* mutant, Chs3 puncta were similar to that of the wild type. This suggests exomer complexes associated with different ChAPs paralogs may have different effects on Chs3 traffic. We hypothesized that exomer containing the Chs6 and/or Bch2 paralogs may strictly act as a cargo receptor whereas the exomer containing Bch1 and/or Bud7 paralogs may have more general effects on traffic, as described above for AAPs.

To test this hypothesis, we explored the effect of the exomer mutants on the localization of $Chs3^{L24A}$ mutant protein which cannot bind the AP-1 complex (25). We found that *chs5Δ* cells expressing $Chs3^{L24A}$ were sensitive to calcofluor white, whereas *chs6Δ* cells

expressing Chs3$^{L24A}$ were moderately resistant to the same calcofluor concentration (Figure 6B). This suggests that in cells lacking Chs5, Chs3$^{L24A}$ reaches the cell surface, while in cells lacking Chs6 Chs3$^{L24A}$ does not reach the plasma membrane. As an independent confirmation, we monitored the localization of Chs3$^{L24A}$-GFP in *chs5Δ*, *chs6Δ bch2Δ* and *bch1Δ bud7Δ* cells. We found Chs3$^{L24A}$-GFP on the cell surface in *chs5Δ* and *bch1Δ bud7Δ* cells but not in *chs6Δ bch2Δ* cells, indicating that the two ChAP paralogous pairs play different roles in Chs3 traffic (Figure S8B).

We sought to explore this hypothesis further by examining the localization of Chs5-Chs3 BIFC complexes in different ChAPs mutant backgrounds. We hypothesized that if complexes containing Chs6/Bch2 were exclusively required for cargo loading in exocytic vesicles then the formation of the Chs5-Chs3 BIFC complexes could be able to bypass this requirement. Surprisingly, we found that Chs5-Chs3 BIFC complexes localized along the cell surface in both *chs6Δ bch2Δ* or *bch1Δ bud7Δ* cells (Figure 6C, S8A). However, these BIFC complexes could not reach the PM in the absence of Chs7 (*chs7Δ* strain), a specific chaperon implicated in a Chs3-exocytic step prior to exomer complex function (37). This suggests that, under this condition, complexes containing only Bch1/Bud7 are competent for exocytosis, and that exocytosis may not be the only role of exomer containing Chs6 and Bch2. Consistent with these findings, we found that the concomitant expression of Chs5-VC and Chs3-VN was able to restore calcofluor white sensitivity to *chs6Δ* (Figure 6D). Interestingly, the Chs5-Chs3 BIFC complexes were conspicuously absent from the neck region in both double mutants, *chs6Δ bch2Δ* and *bch1Δ bud7Δ*, consistent with a lower polarization of the protein similar to the localization observed for the Chs3$^{L24A}$ protein, which is unable to bind the AP-1 complex (Figure S8A).

One explanation for these phenotypes is that the artificially stable Chs3-Chs5 dimer induced by BIFC tags prevents AP-1 from retaining Chs3 in the TGN and therefore the protein can reach the PM without Chs6 or Bch1/Bud7 following an alternative route (27). To test if the converse could be true, we tested the effect of the formation of Apl4-Chs3 BIFC complexes on global Chs3 localization. We found Apl4-Chs3 BIFC complexes were only detected as intracellular dots, consistent with the intracellular localization of the AP-1 complex (Figure 6E, upper panel). The formation of these complexes was highly specific because they were clearly altered in the absence of Gga2 (Figure 6E), a finding that clearly agrees with the proposed role for GGAs in the recruitment of AP-1 to the TGN (6). More important, cells expressing these BIFC complexes were moderately resistant to calcofluor, indicating that artificial stable interaction of Chs3 with AP-1 reduced the exit of Chs3 to the plasma membrane (Figure 6E, lower panel).

Altogether our results suggest that the exomer and AP-1 complexes can compete for some cargoes in *S. cerevisiae*, such as Chs3, but not others such as AAPs. These findings may be highly relevant and influence our understanding of how protein sorting at the TGN (see discussion) may have evolved.

### Exploring the physiological relationship between the exomer and AP-1 complexes in *Candida albicans*.

These multiple lines of evidence support the idea of a TGN niche in where exomer and AP-1 complexes maintain competitive and regulated relationships between themselves and with respect to their cargoes. Thus, we sought to analyze whether these relationships have been conserved along evolution. Considering the evolutionary distribution of the exomer complex (65), we decided to analyze this relationship in *Candida albicans* where both complexes exist. Given the effect of exomer on polarized exocytosis in *Saccharomyces cerevisiae*, we examined filamentous growth which strongly depends on polarized exocytosis. We examined the filamentous growth of cells lacking exomer and AP-1 in liquid (Figure 7A,B) and on different solid media (Figure 7C). Surprisingly, loss of exomer only weakly affected filamentous growth whereas the AP-1 complex was indispensable for hyphal formation on solid media and its absence strongly reduced the rate of hyphal growth in liquid media. However, exomer deletion only partially altered the morphology of filaments growing on solid and in liquid media, and slightly reduces hyphal growth in liquid media. Interestingly, the double mutant showed additive phenotypes, with stronger alterations in colony morphology and a lower hyphal extension rate in liquid media. These results highlight the significant differences between the role of the exomer and AP-1 complexes in yeast or hyphal cells, and suggest that the AP-1 complex has an important role in maintaining polarity during mycelial growth.

## DISCUSSION

### Exomer facilitates the polarized delivery of several proteins to the PM.

The TGN is a major platform for the intracellular sorting of proteins where anterograde and recycling pathways converge (3, 66). Surprisingly, even in yeast, the mechanisms for protein sorting to the PM remain unclear (2). Some years ago, the discovery of exomer as an adaptor complex at the TGN, required for the delivery of Chs3 to the PM (17, 21), opened a pathway to study these mechanisms. However, the number of proteins that depend on exomer for their transport is limited, this observation was striking given the evolutionary maintenance of this sophisticated machinery. Moreover, the phenotypes of mutants lacking exomer, as well as the range of its genetic interaction, suggested additional roles in protein trafficking (21, 42).

The characterization of the sensitivity of exomer mutants to ammonium ((21) and this work) expands the previously reported role of exomer in protein traffic regulation. Here, we have shown that the ammonium sensitivity of exomer mutants is linked to the absence of the unique scaffold Chs5 or the pair of ChAPs Bch1/Bud7, but not to the absence of the other pair of ChAPs Chs6/Bch2, which has been described as cargo adaptor for the Chs3 and Pin2 proteins (22, 23). This suggests additional functions for exomer containing Bch1/Bud7 that are independent of the cargo binding ChAPs.

Our work unequivocally links the ammonium hypersensitivity of the exomer mutant *chs5Δ* to a deficient uptake of tryptophan. Still, our results also suggest that the absence of exomer affects the uptake of other amino acids, based on the partial alleviation of *chs5Δ* ammonium

sensitivity by the *LEU2* gene, or the altered sensitivity to several amino acid analogs. These defects on amino acid uptake are not caused by deficient signaling through the major signaling pathways involved in nitrogen assimilation. Rather, the ammonium sensitivity is directly linked to defective traffic of the tryptophan permease Tat2 in the *chs5Δ* mutant. This traffic defect is shared with the Mup1 permease and the sodium ATPase Ena1 (42). Therefore, our results highlight the involvement of exomer in the polarized traffic of these three proteins, and likely other transporters. This specific function in polarized transport explains why these proteins have not been previously linked to exomer function, since their transport to the plasma membrane is not blocked in the absence of exomer and the defects in polarization, much more discrete, were only detectable after the use of regulatable promoters. Therefore, our work enlarges the spectrum of proteins that rely on exomer for polarized transport. Moreover, the results presented here link this transport to the Bch1/Bud7 pair of ChAPs. These subunits lack the cargo binding activity of the Chs6/Bch2 (22, 23), suggesting that exomer may also contribute to the transport of proteins through its action in coat assembly in addition to its direct role as cargo adaptor. Since Bch1/Bud7 are less divergent from the ChAP representative found in the root of the fungal evolutionary tree, this may suggest this coat function is the ancestral role of the complex (29, 65).

### Exomer contributes to late endosomal traffic of several proteins through its functional relationship with clathrin adaptor complexes.

Our results show that *chs5Δ* disrupts not only the anterograde transport of Tat2 and Mup1 to the PM but also their traffic to the vacuole. This defect is consistent with the overall alterations of the TGN dynamics associated with the modified recruitment of clathrin adaptor complexes at TGN membranes in the absence of exomer. Notably, a similar cooperation between exomer and clathrin adaptors was previously reported in *S. pombe* (30). The deletion of the GGA complex suppressed both the ammonium sensitivity and the tryptophan requirement of the *chs5Δ* mutant. This most likely occurred by reducing Tat2 traffic to the vacuole, thereby restoring its delivery to the plasma membrane (36). Surprisingly, the absence of the AP-1 complex had only a marginal effect on *chs5Δ* phenotypes linked to tryptophan transport, suggesting that AP-1 is not linked to Tat2 traffic. Interestingly, exomer does not seem to affect the early endosomal recycling of Ta2 that is mediated by Rcy1 (55) because the effects of the absence of Rcy1 and Chs5 are additive. In addition, the deletions of *GGA1* or *GGA2* have opposite effects on the ammonium sensitivity of the *rcy1Δ* or *chs5Δ* mutants. Altogether, these results indicate that the absence of exomer affects the late endosomal traffic of Tat2 without affecting its Rcy1-dependent early endosomal recycling (55).

Exomer and clathrin adaptor complexes localize and mediate sorting decisions at the TGN, but also rely on the function of Arf1 GTPase for proper functioning (21, 67). Our results support a model where both exomer and clathrin adaptor complexes would compete for Arf1 based on several lines of evidence. The absence of exomer altered the dynamics of the clathrin adaptor complexes similar to previously reported effects of Pik1/Frq1 overexpression, which is thought to upregulate Arf1 activity (6). In agreement with this evidence, the overexpression of Gga2, which may reduce available levels of Arf1, reduced the effective recruitment of Chs5 to the TGN membranes (Figure S7A). In

addition, overexpression of Arf1 or Sec7 increased chitin synthesis, which is dependent on the presence of a functional exomer, in clear agreement with the regulatory role on exomer function proposed for Arf1 (17, 21, 27). Moreover, this model is also compatible with the action of exomer as an inhibitor of Arf-GAP (GTPase activating protein) activity, as previously proposed (20). Accordingly, overexpression of Arf1/Sec7 did not suppress the chitin synthesis defect associated with the *chs5Δ* mutant. By contrast, depletion of Arf1 or Sec7 effectively suppressed the *chs5Δ*-associated phenotypes, most likely by disrupting clathrin-mediated TGN-endosome traffic (27). Interestingly, overexpression of Sec7 alleviated partially the ammonium sensitivity and the tryptophan requirement of the *chs5Δ* mutant, indicating that Chs3 and Tat2 may follow different itineraries from the TGN.

One unexpected finding of this work is the observation that the polarized delivery of Chs3 is unaffected by the absence of Arf1. This is surprising because polarized delivery of Chs3 depends on the presence of a functional exomer, which should be disrupted when Arf1 is depleted. This result is indicative of the assembly of a functional exomer complex despite the strong morphological alteration of the TGN in the *arf1Δ* mutant. This somehow contradicts previous indirect observations suggesting that Arf1 is required for exomer assembly (17, 21). Whether this observation is explained by the function of Arf2 or other GTPase still remains to be established.

Altogether our results, together with those previously reported (30), show that in addition to the described role of exomer in the anterograde transport of proteins exomer also contributes to the late endosomal traffic of multiple proteins by facilitating the proper functioning of the clathrin adaptor complexes. This function appears to be independent of the cargo binding activity of exomer, and may vastly increase the number of proteins known to depend on exomer for localization.

### Exomer and AP-1 complexes compete for a subset of cargoes.

An interesting reported here observation is the differential effect of the AP-1 complex on the traffic of exomer-dependent proteins. Our phenotypic analysis showed that deletion of AP-1 complex has little effect on Tat2 traffic in the *chs5Δ* mutants, which is similar to prior reports about Ena1 (42). By contrast, the absence of AP-1 efficiently reroutes Chs3, as well as the other bona fide cargoes, Fus1 and Pin2, to the PM in the absence of exomer (18, 19). This can be simply explained by the physical interaction between these cargoes and both the exomer and AP-1 complexes as it has been shown for Chs3 (25, 26). Our *in vivo* results favor a mechanistic model in which exomer and AP-1 compete for cargoes, since the artificially increased interaction between Chs3 and Chs5 through the BIFC system allows Chs3 traffic to PM avoiding the TGN-retention of Chs3 mediated by AP-1 in *chs6Δ* and *bch1Δ bud7Δ* mutants. Moreover, tighter binding of Chs3 to AP-1 using the BIFC system also reduced Chs3 traffic to the PM (Figure 6).

In addition to the direct competition between exomer and AP-1 for cargoes, we propose that competition for Arf1 also contributes to their complex interaction. Exomer and CCV are assembled at the TGN in close proximity ((58), and this work), and both utilize Arf1 (Figure 7D). Moreover, exomer is strictly required for the PM delivery of a restricted number of cargoes that are recycled to the TGN through their physical interaction with

the AP-1 complex (Figure 7E). However, exomer also facilitates the polarized delivery of other proteins that recycle independently of AP-1. Additionally, exomer contributes to the proper assembly of the clathrin adaptor complexes that facilitate late endosomal traffic of multiple proteins. Functional disruption of clathrin adaptors complexes reroutes proteins into alternative non-polarized ways to the PM. Our results also discriminate between the functions of the GGA and AP-1 complexes at the TGN in *S. cerevisiae*, a subject still under debate. The role of AP-1 in *S. cerevisiae* appears limited, affecting only a restricted number of cargoes that are recycled by this complex through their direct binding. The GGA complex appears to perform more general functions in the organization of the TGN. This occurs independently of the specific recognition of the cargoes (6) thus affecting the late endosomal traffic of several proteins (68–70). This view is similar to what has been proposed for animal cells, in which AP-1 would have a distinct role in the protein recycling that is not shared with GGAs (71).

The many functional connections between exomer and AP-1 found in yeasts help to raise the interesting question of whether these are evolutionarily conserved relationships. Our work with *C. albicans* (Figure 7A–C and (29)) indicates that while exomer contributes to the polarization of Chs3 and only displays a secondary role in filamentous growth, AP-1 is pivotal for this hyperpolarized process (Figure 7F). More broadly, the absence of AP-1 is lethal in filamentous fungi (72). However, all exomer mutants characterized are fully viable (29, 30) (M. Riquelme, personal communication), suggesting that the functional interconnection between exomer and AP-1 may be limited to yeast cells within the fungal lineage. The AP-1 complex is conserved in eukaryotes (73), but exomer appears to be fungal specific (65), evidence that is consistent with the major role of AP-1 in polarized traffic in animal cells (74). Therefore, our results reflect the general idea that polarity determinants (2), and thus the mechanism of sorting at the TGN, are highly diverse, coexisting mechanisms based on cargo adaptor complexes together with others based on protein partitioning between micro-domains, with exomer somehow exerting both functions in yeast depending on the cargo to be sorted.

## Supplementary Material

Refer to Web version on PubMed Central for supplementary material.

## ACKNOWLEDGMENTS

We thank A. Spang, J. Ariño and S. Moreno for strains and reagents and for the many useful discussions that took place throughout this work and to E. Keck for the editorial correction of the manuscript. We especially acknowledge the initial work carried out by M. Berroa on *C. albicans*. CAP was supported by a University of Salamanca (USAL) predoctoral fellowship, an EMBO short-term fellowship and an USAL Grant for Excellence; NS was supported by a FPU fellowship from the Spanish Ministry of Education. Work at the CR laboratory was supported by grants BFU2017-84508-P from the CICYT/FEDER program (Ministerio de Economía, Industria y Competitividad, Gobierno de España) and SA116G19 from Consejería de Educación, Junta de Castilla y León. JMM laboratory was supported by grants RTC-2017-6468-2-AR and BIO2016-77776-P (Ministerio de Economía, Industria y Competitividad, Gobierno de España) and work by MCD was supported by the National Institutes of Health (USA) grant R01 GM092741 and by funds from the Michigan Protein Folding Disease Initiative. CR also thanks the financial support awarded to the Institute of Biological and Functional Genomics (IBFG) (CLU-2017-03) provided by the Junta de Castilla y León through the program “Escalera de Excelencia”, co-financed by the P.O. FEDER of Castilla y León 14-20.

## ABBREVIATIONS

| | |
|---|---|
| **TGN** | *trans* Golgi network |
| **PM** | plasma membrane |
| **PVC** | pre-vacuolar compartment |
| **EE** | early endosomes |
| **MVB** | multi vesicular body |
| **ER** | Endoplasmic reticulum |
| **BIFC** | Bimolecular fluorescence complementation |
| **CCV** | clathrin coated vesicles |
| **AP-1** | clathrin adaptor complex-1 |
| **GGA** | Golgi-localizing, Gamma-adaptin ear homology, ARF-binding proteins |
| **PtdIns(4)P** | Phosphatidylinositol 4-phosphate |
| **ChAP** | Chs5-Arf1 binding proteins |
| **PCR** | polymerase chain reaction |
| **ORF** | open reading frame |
| **GFP** | green fluorescent protein |
| **HA** | Human influenza hemagglutinin epitope |
| **YEP** | yeast extract and peptone medium |
| **YEPD** | yeast extract, peptone and dextrose medium |
| **SD** | synthetic defined medium |
| **YNB-N-aa** | yeast nitrogen base without nitrogen and without amino acids |
| **CW** | calcofluor white |
| **IC50** | half maximal inhibitory concentration |
| **$OD_{600}$** | optical density at wavelength of 600nm |
| **TCA** | trichloroacetic acid |
| **DTT** | dithiothreitol |
| **SDS** | sodium dodecyl sulfate |

| | |
|---|---|
| **BSA** | bovine serum albumin |
| **RT** | room temperature |
| **O/N** | overnight |
| **3-AT** | 3-aminotriazole |
| **AzC** | L-azetidin-2-carboxilate |
| **AAP** | amino acid permease |
| **SPS** | Ssy1p-Ptr3p-Ssy5 cellular sensor |
| **NCR** | Nitrogen Catabolite Repression |
| **TORC1** | target of rapamycin kinase complex I |
| **GEF** | guanine nucleotide exchange factor |
| **GAP** | GTPase activating protein |
| **mR2** | mRuby2 epitope |
| **VC** | C terminus fragment of Venus fluorescent protein |
| **VN** | N terminus fragment of Venus fluorescent protein |
| **ROI** | Region of interest |

## REFERENCES


1. De Matteis MA, and Luini A (2008) Exiting the Golgi complex. Nat Rev Mol Cell Biol 9, 273–284 [PubMed: 18354421]
2. Bonifacino JS (2014) Adaptor proteins involved in polarized sorting. J Cell Biol 204, 7–17 [PubMed: 24395635]
3. Guo Y, Sirkis DW, and Schekman R (2014) Protein sorting at the trans-Golgi network. Annu Rev Cell Dev Biol 30, 169–206 [PubMed: 25150009]
4. Robinson MS (2015) Forty Years of Clathrin-coated Vesicles. Traffic 16, 1210–1238 [PubMed: 26403691]
5. Traub LM (2005) Common principles in clathrin-mediated sorting at the Golgi and the plasma membrane. Biochem Biophys Acta 1744, 415–437 [PubMed: 15922462]
6. Daboussi L, Costaguta G, and Payne GS (2012) Phosphoinositide-mediated clathrin adaptor progression at the trans-Golgi network. Nat Cell Biol 14, 239–248 [PubMed: 22344030]
7. Becuwe M, and Leon S (2014) Integrated control of transporter endocytosis and recycling by the arrestin-related protein Rod1 and the ubiquitin ligase Rsp5. eLife 3
8. Scott PM, Bilodeau PS, Zhdankina O, Winistorfer SC, Hauglund MJ, Allaman MM, Kearney WR, Robertson AD, Boman AL, and Piper RC (2004) GGA proteins bind ubiquitin to facilitate sorting at the trans-Golgi network. Nature cell biology 6, 252–259 [PubMed: 15039776]
9. Deng Y, Guo Y, Watson H, Au WC, Shakoury-Elizeh M, Basrai MA, Bonifacino JS, and Philpott CC (2009) Gga2 mediates sequential ubiquitin-independent and ubiquitin-dependent steps in the trafficking of ARN1 from the trans-Golgi network to the vacuole. The Journal of biological chemistry 284, 23830–23841 [PubMed: 19574226]
10. Stringer DK, and Piper RC (2011) A single ubiquitin is sufficient for cargo protein entry into MVBs in the absence of ESCRT ubiquitination. J Cell Biol 192, 229–242 [PubMed: 21242292]

11. Ha SA, Torabinejad J, DeWald D,B, Wenk MR, Lucas t. L., De Camilli P, Newitt RA, Aebersold R, and Nothwehr SF (2003) The synaptojanin-like protein Inp53/Sjl3 functions with clathrin in a yeast TGN-to-endosome pathway distinct from the GGA protein-dependent pathway. Mol Biol Cell 14, 1319–1333 [PubMed: 12686590]
12. Marcusson EG, Horazdovsky BF, Cereghino JL, Gharakhanian E, and Emr SD (1994) The sorting receptor for yeast vacuolar carboxypeptidase Y is encoded by the VPS10 gene. Cell 77, 579–586 [PubMed: 8187177]
13. Yeung BG, and Payne GS (2001) Clathrin interactions with C-terminal regions of the yeast AP-1 beta and gamma subunits are important for AP-1 association with clathrin coats. Traffic 2, 565–576 [PubMed: 11489214]
14. Gall WE, Geething NC, Hua Z, Ingram MF, Liu K, Chen SI, and Graham TR (2002) Drs2p-dependent formation of exocytic clathrin-coated vesicles in vivo. Curr Biol 17, 1623–1627
15. Santos B, and Snyder M (1997) Targeting of chitin synthase 3 to polarized growth sites in yeast requires Chs5p and Myo2p. J. Cell Biol 136, 95–110 [PubMed: 9008706]
16. Ziman M, Chuang JS, Tsung M, Hamamoto S, and Schekman R (1998) Chs6p-dependent anterograde transport of Chs3p from the chitosome to the plasma membrane in Saccharomycces cerevisiae. Mol. Biol. Cell 9, 1565–1576 [PubMed: 9614194]
17. Wang CW, Hamamoto S, Orci L, and Schekman R (2006) Exomer: A coat complex for transport of select membrane proteins from the trans-Golgi network to the plasma membrane in yeast. J. Cell Biol 174, 973–983 [PubMed: 17000877]
18. Barfield RM, Fromme JC, and Schekman R (2009) The exomer coat complex transports Fus1p to the plasma membrane via a novel plasma membrane sorting signal in yeast. Mol. Biol. Cell 20, 4985–4996 [PubMed: 19812245]
19. Ritz AM, Trautwein M, Grassinger F, and Spang A (2014) The prion-like domain in the exomer-dependent cargo Pin2 serves as a trans-Golgi retention motif. Cell Rep 10, 249–260
20. Paczkowski JE, Richardson BC, Strassner AM, and Fromme JC (2012) The exomer cargo adaptor structure reveals a novel GTPase-binding domain. EMBO J 31, 4191–4203 [PubMed: 23000721]
21. Trautwein M, Schindler C, Gauss R, Dengjel J, Hartmann E, and Spang A (2006) Arf1p, Chs5p and the ChAPs are required for export of specialized cargo from the Golgi. EMBO J 25, 943–954 [PubMed: 16498409]
22. Paczkowski JE, and Fromme JC (2014) Structural basis for membrane binding and remodeling by the exomer secretory vesicle cargo adaptor. Dev Cell 30, 610–624 [PubMed: 25203211]
23. Huranova M, Muruganandam G, Weiss M, and Spang A (2016) Dynamic assembly of the exomer secretory vesicle cargo adaptor subunits. EMBO Rep 17, 202–219 [PubMed: 26742961]
24. Rockenbauch U, Ritz AM, Sacristan C, Roncero C, and Spang A (2012) The complex interactions of Chs5p, the ChAPs, and the cargo Chs3p. Mol Biol Cell 23, 4404–44015
25. Starr TL, Pagant S, Wang CW, and Schekman R (2012) Sorting Signals That Mediate Traffic of Chitin Synthase III between the TGN/Endosomes and to the Plasma Membrane in Yeast. PloS One 7, e46386. doi: 46310.41371/ [PubMed: 23056294]
26. Weiskoff AM, and Fromme JC (2014) Distinct N-terminal regions of the exomer secretory vesicle cargo Chs3 regulate its trafficking itinerary. Front Cell Dev Biol 2:47, doi: 10.3389/fcell.2014.00047 [PubMed: 25364754]
27. Valdivia RH, Baggot D, Chuang JS, and Schekman R (2002) The yeast Clathrin adaptor protein complex 1 is required for the efficeint retention of a subset of late Golgi membrane proteins. Dev. Cell 2, 283–294 [PubMed: 11879634]
28. Zanolari B, Rockenbauch U, Trautwein M, Clay L, Barral Y, and Spang A (2011) Transport to the plasma membrane is regulated differently early and late in the cell cycle in Saccharomyces cerevisiae. J. Cell Sci 124, 1055–1066 [PubMed: 21363887]
29. Anton C, Valdez Taubas J, and Roncero C (2018) The Functional Specialization of Exomer as a Cargo Adaptor During the Evolution of Fungi. Genetics 208, 1483–1498 [PubMed: 29437703]
30. Hoya M, Yanguas F, Moro S, Prescianotto-Baschong C, Doncel C, de León N, Curto MÁ, Spang A, and Valdivieso MH (2017) Traffic Through the Trans-Golgi Network and the Endosomal System Requires Collaboration Between Exomer and Clathrin Adaptors in Fission Yeast. Genetics 205, 673–690 [PubMed: 27974503]

31. Rose MD, Wisnton F, and Hieter P (1990) Methods in Yeast Genetics: A Laboratory Course Manual, Cold Spring Harbor Laboratory Press, New York
32. Goldstein AL, and McCusker JH (1999) Three new dominant drug resistance cassettes for gene disruption in Saccharomyces cerevisiae. Yeast 15, 1541–1553 [PubMed: 10514571]
33. Longtine MS, McKenzie A. r., Demarini DJ, Shah NG, Wach A, Brachat A, Philippsen P, and Pringle JR (1998) Additional modules for versatile and economical PCR-based gene deletion and modification in Saccharomyces cerevisiae. Yeast. 14, 953–961 [PubMed: 9717241]
34. Sato M, Dhut S, and Toda T (2005) New drug-resistant cassettes for gene disruption and epitope tagging in Schizosaccharomyces pombe. Yeast 22, 582–591
35. Stuckey S, Mukherjee K, and Storici F (2011) In vivo site-specific mutagenesis and gene collage using the delitto perfetto system in yeast Saccharomyces cerevisiae. Methods Mol Biol 745, 173–191 [PubMed: 21660695]
36. Hachiro T, Yamamoto T, Nakano K, and Tanaka K (2013) Phospholipid flippases Lem3p-Dnf1p and Lem3p-Dnf2p are involved in the sorting of the tryptophan permease Tat2p in yeast. J Biol Chem 288, 3594–3608 [PubMed: 23250744]
37. Trilla JA, Duran A, and Roncero C (1999) Chs7p, a new protein involved in the control of protein export from the endoplasmic reticulum that is specifically engaged in the regulation of chitin synthesis in Saccharomyces cerevisiae. J. Cell Biol 145, 1153–1163 [PubMed: 10366589]
38. Hung CW, Martínez-Márquez JY, FT J, and Duncan MC (2018) A simple and inexpensive quantitative technique for determining chemical sensitivity in Saccharomyces cerevisiae. Sci Rep 8, 11919 [PubMed: 30093662]
39. Sung MK, and Huh WK (2007) Bimolecular fluorescence complementation analysis system for in vivo detection of protein-protein interaction in Saccharomyces cerevisiae. Yeast 24, 767–775 [PubMed: 17534848]
40. Arcones I, and Roncero C (2016) Monitoring chitin deposition during septum assembly in budding yeast. Methods Mol Biol 1369, 59–72 [PubMed: 26519305]
41. Vicent I, Navarro A, Mulet JM, Sharma S, and Serrano R (2015) Uptake of inorganic phosphate is a limiting factor for Saccharomyces cerevisiae during growth at low temperatures. FEMS Yeast Res 15, fov008 [PubMed: 25725023]
42. Anton C, Zanolari B, Arcones I, Wang C, Mulet JM, Spang A, and Roncero C (2017) Involvement of the exomer complex in the polarized transport of Ena1 required for Saccharomyces cerevisiae survival against toxic cations. Mol Biol Cell 28, 3672–3685 [PubMed: 29021337]
43. Hess DC, Lu W, Rabinowitz JD, and Botstein D (2006) Ammonium toxicity and potassium limitation in yeast. PLoS Biol 4, e351 [PubMed: 17048990]
44. Schmidt A, Hall MN, and Koller A (1994) Two FK506 resistance-conferring genes in Saccharomyces cerevisiae, TAT1 and TAT2, encode amino acid permeases mediating tyrosine and tryptophan uptake. Mol Cell Biol 14, 6597–6606 [PubMed: 7523855]
45. Ljungdahl PO, and Daignan-Fornier B (2012) Regulation of amino acid, nucleotide, and phosphate metabolism in Saccharomyces cerevisiae. Genetics 190, 885–929 [PubMed: 22419079]
46. Ljungdahl PO, Gimeno CJ, Styles CA, and Fink GR (1992) SHR3: a novel component of the secretory pathawy specifically required for localization of aminoacid permeasesin yeast. Cell 71, 463–478 [PubMed: 1423607]
47. Kanazawa S, Driscoll M, and Struhl K (1992) ATR1, a Saccharomyces cerevisiae gene encoding a transmembrane protein required for aminotriazole resistance. Mol Cell Biol 8, 664–673
48. Wada M, Okabe K, Kataoka M, Shimizu S, Yokota A, and Takagi H (2008) Distribution of L-azetidine-2-carboxylate N-acetyltransferase in yeast. Biosci Biotechnol Biochem 72, 582–586 [PubMed: 18256475]
49. Falco SC, and Dumas KS (1985) Genetic analysis of mutants of Saccharomyces cerevisiae resistant to the herbicide sulfometuron methyl. Genetics 109, 21–35 [PubMed: 3881312]
50. Larimer FW, Ramey DW, Lijinsky W, and Epler JL (1978) Mutagenicity of methylated N-nitrosopiperidines in Saccharomyces cerevisiae. Mutat Res 57, 155–161 [PubMed: 351388]
51. González A, Shimobayashi M, Eisenberg T, Merle DA, Pendl T, Hall MN, and Moustafa T (2015) TORC1 promotes phosphorylation of ribosomal protein S6 via the AGC kinase Ypk3 in Saccharomyces cerevisiae. PLos One 10, e0120250 [PubMed: 25767889]

52. Zhang W, Du G, Zhou J, and Chen J (2018) Regulation of Sensing, Transportation, and Catabolism of Nitrogen Sources in Saccharomyces cerevisiae. Microbiol Mol Biol Rev 82, e00040–00017 [PubMed: 29436478]

53. Beck T, Schmidt A, and Hall MN (1999) Starvation induces vacuolar targeting and degradation of the tryptophan permease in yeast. J Cell Biol 146, 1227–1238 [PubMed: 10491387]

54. Menant A, Barbey R, and homas D (2006) Substrate-mediated remodeling of methionine transport by multiple ubiquitin-dependent mechanisms in yeast cells. EMBO J 25, 4436–4447 [PubMed: 16977312]

55. MacDonald C, and Piper RC (2017) Genetic dissection of early endosomal recycling highlights a TORC1-independent role for Rag GTPases. J Cell Biol 216, 3275–3290 [PubMed: 28768685]

56. Copic A, Starr TL, and Schekman R (2007) Ent3p and Ent5p exhibit cargo-specific functions in trafficking proteins between the trans-Golgi network and the endosomes in yeast. Mol. Biol. Cell 18, 1803–1815 [PubMed: 17344475]

57. Abe F, and H. I (2003) Pressure-induced differential regulation of the two tryptophan permeases Tat1 and Tat2 by ubiquitin ligase Rsp5 and its binding proteins, Bul1 and Bul2. Mol Cell Biol, 7566–7584 [PubMed: 14560004]

58. Tojima T, Suda Y, Ishii M, Kurokawa K, and Nakano A (2019) Spatiotemporal dissection of the trans-Golgi network. J Cell Sci 132, jcs231159 [PubMed: 31289195]

59. Whitfield ST, Burston HE, Bean BD, Raghuram N, Maldonado-Báez L, Davey M, Wendland B, and Conibear E (2016) The alternate AP-1 adaptor subunit Apm2 interacts with the Mil1 regulatory protein and confers differential cargo sorting. Mol Biol Cell 27, 588–598 [PubMed: 26658609]

60. Zysnarski CJ, Lahiri S, Javed FT, Martínez-Márquez JY, Trowbridge JW, and Duncan MC (2019) Adaptor protein complex-1 (AP-1) is recruited by the HEATR5 protein Laa1 and its co-factor Laa2 in yeast. J Biol Chem 294, 1410–1419 [PubMed: 30523155]

61. Jian X, Cavenagh M, Gruschus JM, Randazzo PA, and Kahn RA (2010) Modifications to the C-terminus of Arf1 alter cell functions and protein interactions. Traffic 11, 732–742 [PubMed: 20214751]

62. Gaynor EC, Chen CY, Emr SD, and Graham TR (1998) ARF is required for maintenance of yeast Golgi and endosome structure and function. Mol Biol Cell 9, 653–670 [PubMed: 9487133]

63. Richardson BC, McDonold CM, and Fromme JC (2012) The Sec7 Arf-GEF is recruited to the trans-Golgi network by positive feedback. Dev Cell 22, 799–810 [PubMed: 22516198]

64. Roncero C (2002) The genetic complexity of chitin synthesis in fungi. Curr Genet. 41, 367–378 [PubMed: 12228806]

65. Ramirez-Macias I, Barlow LD, Anton C, Spang A, Roncero C, and Dacks JB (2018) Evolutionary cell biologyt traces de rise of exomer complex in Fungi from an ancient eukaryotic component. Sci Rep 8, 11154 [PubMed: 30042439]

66. Day KJ, Casler JC, and Glick BS (2018) Budding Yeast Has a Minimal Endomembrane System. Dev Cell 44, 56–72 [PubMed: 29316441]

67. Graham TR, and Burd CG (2011) Coordination of Golgi functions by phosphatidylinositol 4-kinases. Trends Cell Biol 21, 113–121 [PubMed: 21282087]

68. Bonifacino JS, and Glick BS (2004) The mechanisms of vesicle budding and fusion. Cell. 116, 153–166 [PubMed: 14744428]

69. Buelto D, Hung CW, Aoh QL, Lahiri S, and Duncan MC (2020) Plasma membrane to vacuole traffic induced by glucose starvation requires Gga2-dependent sorting at the trans-Golgi network. Biol Cell 112, 349–367 [PubMed: 32761633]

70. Casler JC, and Glick BS (2020) A microscopy-based kinetic analysis of yeast vacuolar protein sorting. Elife 25, e56844

71. Hirst J, Borner GH, Antrobus R, Peden AA, Hodson NA, Sahlender DA, and Robinson MS (2012) Distinct and overlapping roles for AP-1 and GGAs revealed by the “knocksideways” system. Curr Biol 22, 1711–1716 [PubMed: 22902756]

72. Martzoukou O, Diallinas G, and Amillis S (2018) Secretory Vesicle Polar Sorting, Endosome Recycling and Cytoskeleton Organization Require the AP-1 Complex in Aspergillus nidulans. Genetics 209, 1121–1138 [PubMed: 29925567]

73. Barlow LD, Dacks JB, and Wideman J (2014) From all to (neraly) none. Cell Logist 4, e28114 [PubMed: 24843829]

74. Caceres PS, Gravotta D, Zager PJ, Dephoure N, and Rodriguez-Boulan E (2019) Quantitative proteomics of MDCK cells identify unrecognized roles of clathrin adaptor AP-1 in polarized distribution of surface proteins. Proc Natl Acad Sci USA 116, 11796–11805 [PubMed: 31142645]

75. Enloe B, Diamond A, and Mitchell AP (2000) A single-transformation gene function test in diploid Candida albicans. J Bacteriol 182, 5730–5736 [PubMed: 11004171]

76. Lee S, Lim WA, and Thorn KS (2013) Improved blue, green, and red fluorescent protein tagging vectors for S. cerevisiae. PLos One 8, e67902 [PubMed: 23844123]

77. Sacristan C, Manzano-Lopez J, Reyes A, Spang A, Muniz M, and Roncero C (2013) Dimerization of the chitin synthase Chs3 is monitored at the Golgi and affects its endocytic recycling. Mol Microbiol 90, 252–266 [PubMed: 23926947]

78. Arcones I, Sacristán C, and Roncero C (2016) Maintaining protein homeostasis: early and late endosomal dual recycling for the maintenance of intracellular pools of the plasma membrane protein Chs3. Mol Biol Cell 27, 4021–4032 [PubMed: 27798229]

79. Gola S, Martin R, Walther A, Dünkler A, and Wendland J (2003) New modules for PCR-based gene targeting in Candida albicans: rapid and efficient gene targeting using 100 bp of flanking homology region. Yeast 20, 1339–1347 [PubMed: 14663826]

80. Schaub Y, Dünkler A, Walther A, and Wendland J (2006) New pFA-cassettes for PCR-based gene manipulation in Candida albicans. J Basic Microbiol 46, 416–429 [PubMed: 17009297]

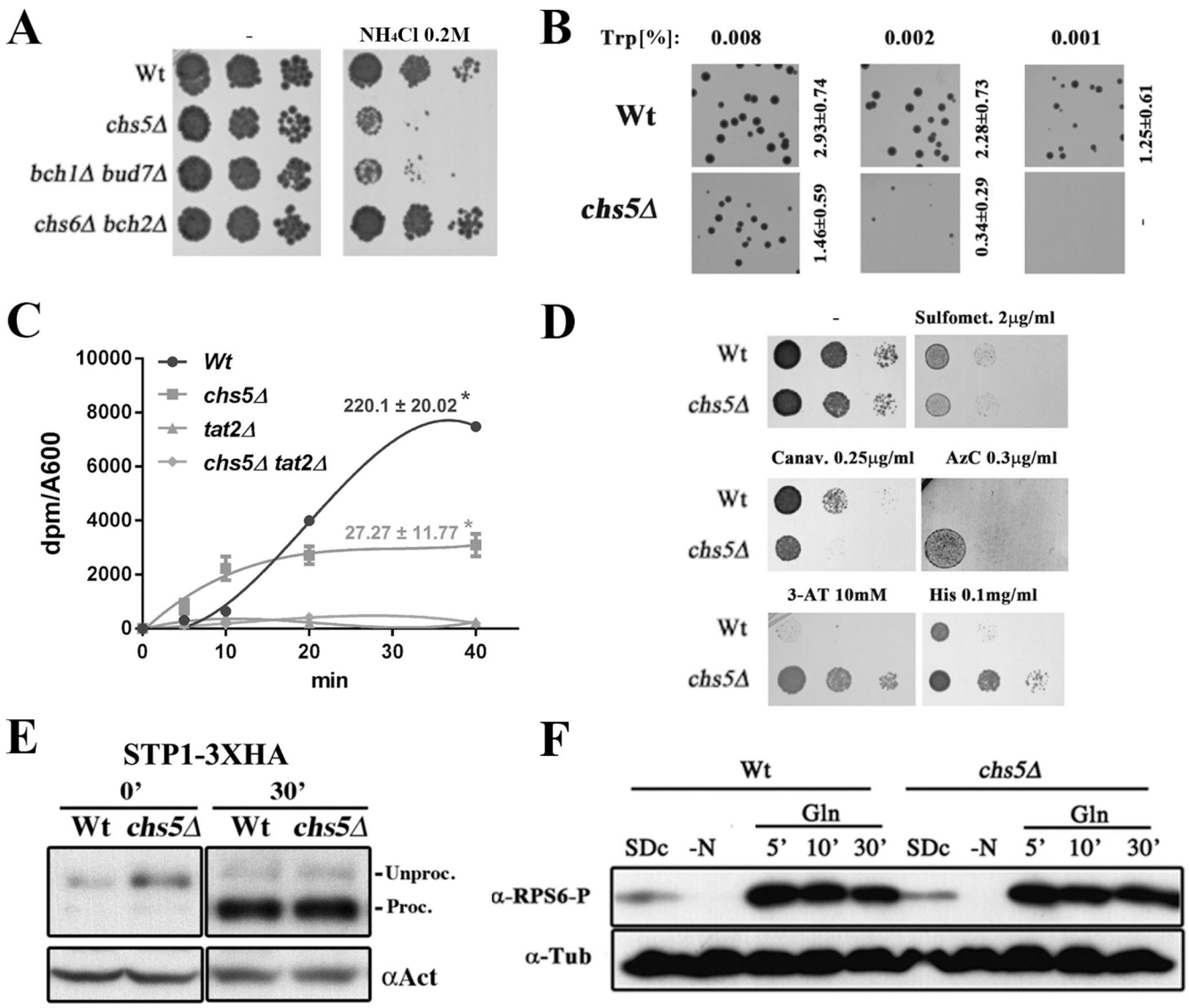


**Figure 1.**

Ammonium sensitivity of the exomer mutants is due to defects in amino acid uptake. (A) Overnight (O/N) cultures of the indicated strains in the W303 genetic background were diluted and plated onto YEPD media supplemented with 0.2 M $NH_4Cl$. Note the similar level of sensitivity of the *chs5Δ* and *bch1Δ/bud7Δ* mutants. (B) O/N cultures of the indicated strains in the W303 background were diluted and spread on synthetic defined media (SD) supplemented with the indicated concentrations of tryptophan. Note that low concentrations (%) of tryptophan (Trp) allowed the wild-type strain to completely grow, but was unable to efficiently support the growth of the *chs5Δ* mutant. The numbers indicate the average diameter ± standard deviation of the colonies growing on the different media quantified using *ImageJ* (Macro3). Also refer to supplemental Figure S1 for additional data on ammonium sensitivity. (C) L-[5-$^3$H]-tryptophan uptake in SD media by the indicated X2180-derived prototrophic strains. Numeric values indicate the incorporation rate (dpm/$A_{600}$/min) calculated as the slope of the linear regression made using 10 to 40 minutes time

points. Note the absence of Trp incorporation in the *tat2Δ* mutants used as the control. (D) Sensitivity of the indicated X2180-derived strains to toxic amino acids analogs. Growth was analyzed in YEPD supplemented with the indicated concentrations of the following analogs: Sulfometuron-metil; L-canavanine; L-azetidin-2-carboxilate (AzC); 3-aminotriazole (3-AT) and L-histidine as indicated. (E) Western blot of the total protein from the cellular extracts of strains carrying *STP1*-3xHA integrated at the chromosomal locus. Cultures starved for 1 hour in YNB-N-aa media were transferred to rich YEPD media and samples were taken at 0 and 30 minutes. Note the similar processing of the Spt1 transcription factor in the wild-type and *chs5Δ* strains. (F) Induction of Rsp6 phosphorylation after adding glutamine. X2180 strains grown on SD complete media were transferred to media lacking a nitrogen source for 1h; glutamine (500 μg/ml) was then added to the media. Note that the kinetics of the phosphorylation induced in the wild type and *chs5Δ* are similar. Phosphorylation was determined by Western blot using a phospho-(Ser/Thr) Akt substrate antibody (#9611s, Cell SignalingTech). Also refer to supplemental Figure S2 for the rationale behind these experiments.

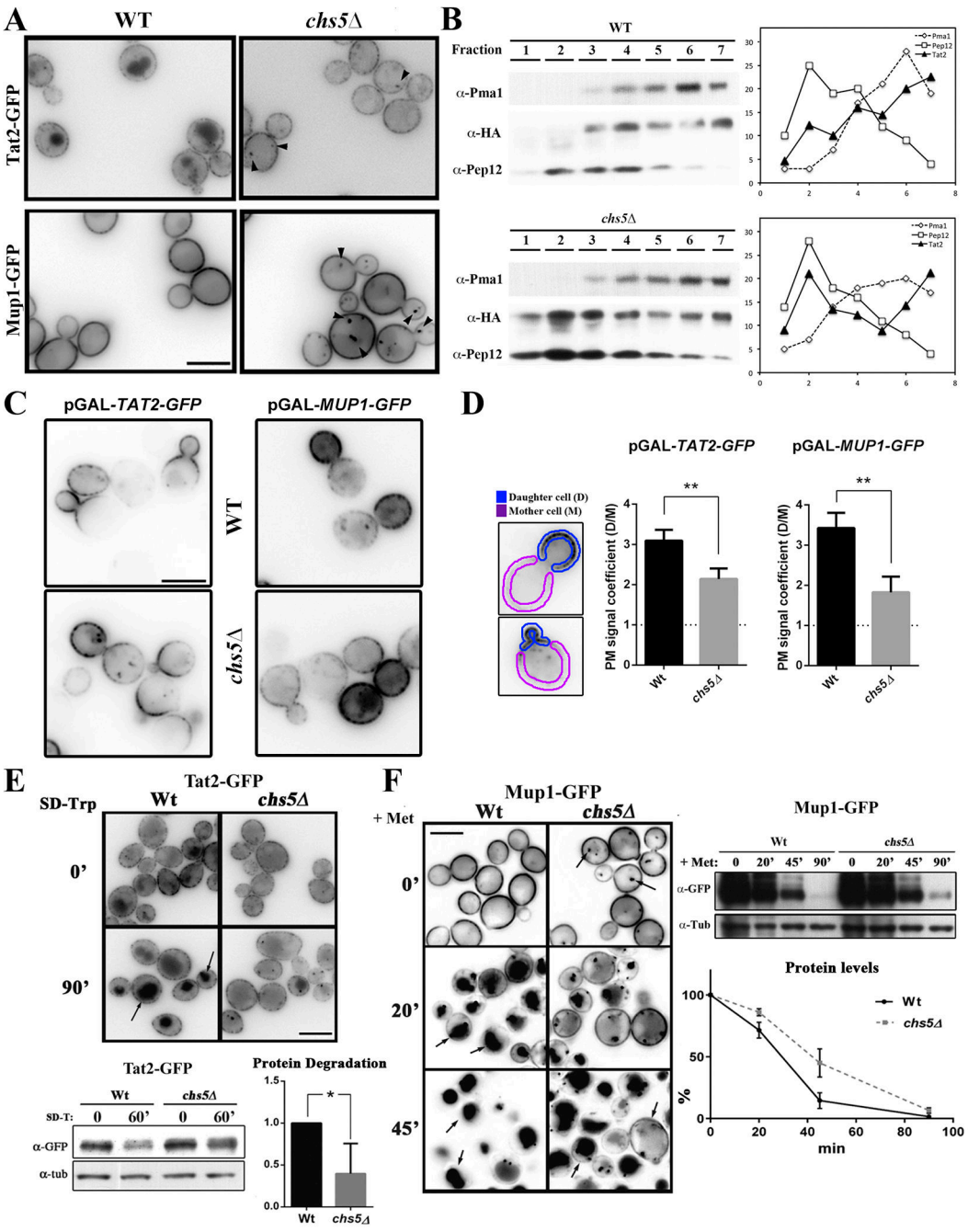


**Figure 2.**

Exomer controls the traffic of several amino acid permeases. (A) Localization of Tat2-GFP and Mup1-GFP under steady state growth conditions in induction media. Note the subtle differences of Tat2 and Mup1 intracellular localization in the exomer mutant and their accumulation at intracellular spots (see arrowheads). (B) Intracellular distribution of Tat2$^{52\text{-}53}$-3xHA in wild-type and *chs5Δ* strains after discontinuous subcellular fractionation. Proteins were visualized by Western blot as described in the Material and Methods section. Graphs on the right represent the percentage of each protein at each fraction. Pma1 and

Pep12 were used as markers for the PM and TGN/endosome fraction respectively. (C) Analysis of the PM anterograde transport of Tat2-GFP and Mup1-GFP, with their gene expression under the control of the GAL1 promoter. In both cases, for pGAL-*TAT2*-GFP and pGAL-*MUP1*-GFP strains, the cells were grown O/N in SD 2 % raffinose media and then transferred to a SD 2% galactose media. In the case of Tat2, and taking in to account the lethality of the lack of Tat2, 0.02% Trp was added to the SD raffinose media and the galactose induction phase was done in a SD media with standard tryptophan concentrations (0.002 %). All images were acquired just one hour after the addition of galactose. (D) Quantitative analysis of the polarization of these proteins along the PM using images from the experiment shown in C. A daughter cell/ mother cell PM signal coefficient was measured following the scheme shown in the left panel (details in Material and Methods section). The horizontal dashed line represents the condition of the lack of polarization of PM protein distribution. (E) Localization and dynamics of Tat2-GFP after the induction of its endocytosis in Trp-depleted media (53). The same experiment was analyzed by Western blot and relative protein degradation after 60 min of induction was calculated from 3 independent experiments (lower panels). (F) Localization and dynamics of Mup1-GFP after the induction of its endocytosis by adding methionine (20 mg/L) (54). The same experiment was analyzed by Western blot and relative protein levels were calculated for each point (lower panel).

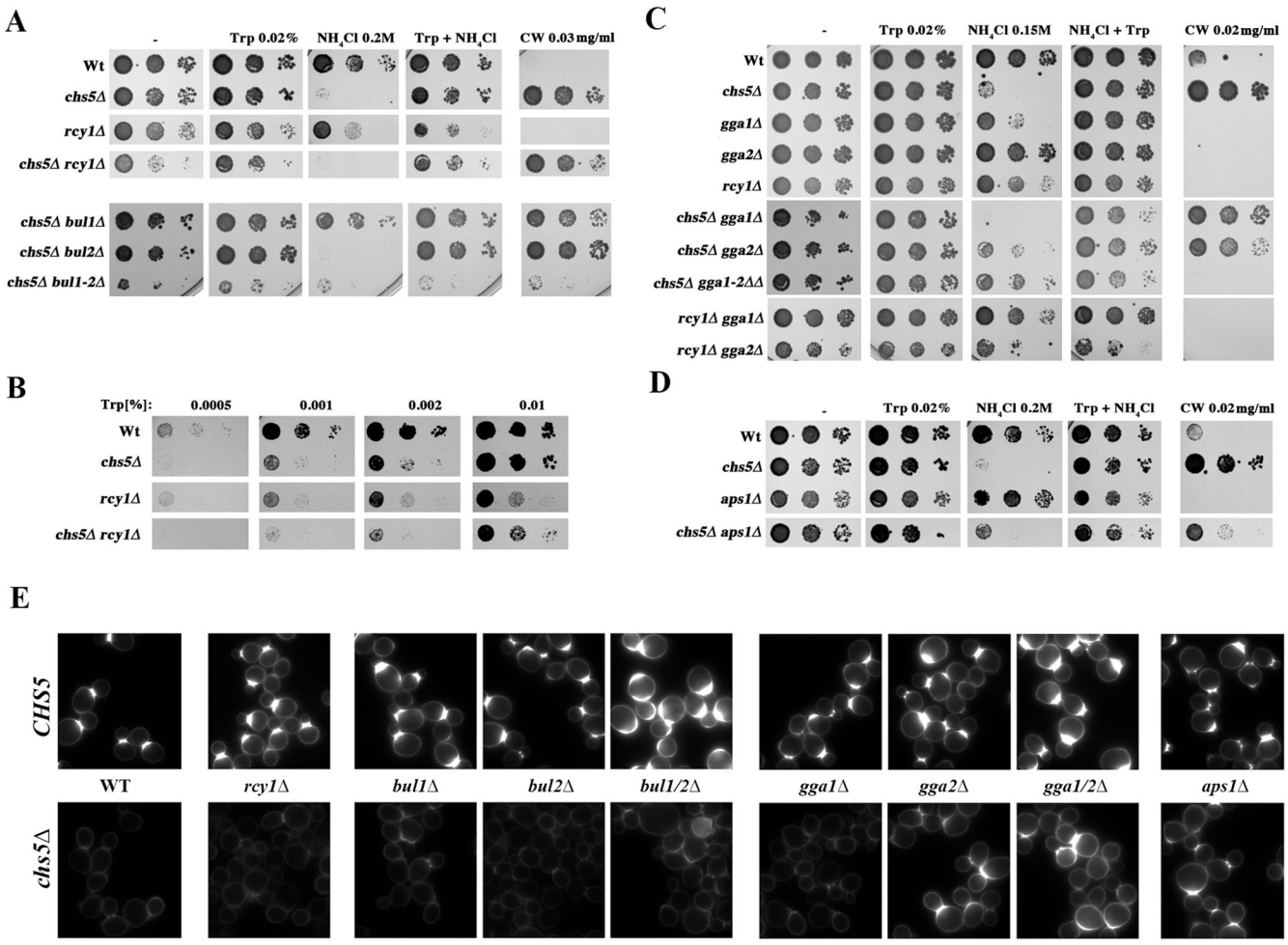


**Figure 3.**

The need for tryptophan and the blockage of chitin synthesis of the *chs5Δ* mutant are differentially suppressed by several mutations affecting TGN traffic. (A) Growth of the indicated strains in YEPD media with the indicated supplements. (B) Growth of the indicated strains in SD w/o Trp media supplemented with the indicated concentrations of Trp. (C, D) Growth of the indicated strains in YEPD media with the indicated supplements. All strains used are W303 derivatives grown O/N in YEPD media, serially diluted and plated onto the indicated media. Each panel represents a single experiment using a unique set of plates; note the slight differences in the growth of similar strains between different panels/experiments. (E) Calcofluor staining of the indicated strains. Cells grown in YEPD media were stained for 1.5 hours with calcofluor (50 μg/ml). Note the reduction in calcofluor staining shown by all *chs5Δ* strains that is partially reverted by *gga2Δ*, *gga1Δ/gga2Δ* and *aps1Δ* concomitant mutations. This result coincides with their higher level of sensitivity to this drug, which is shown in the other figure panels.

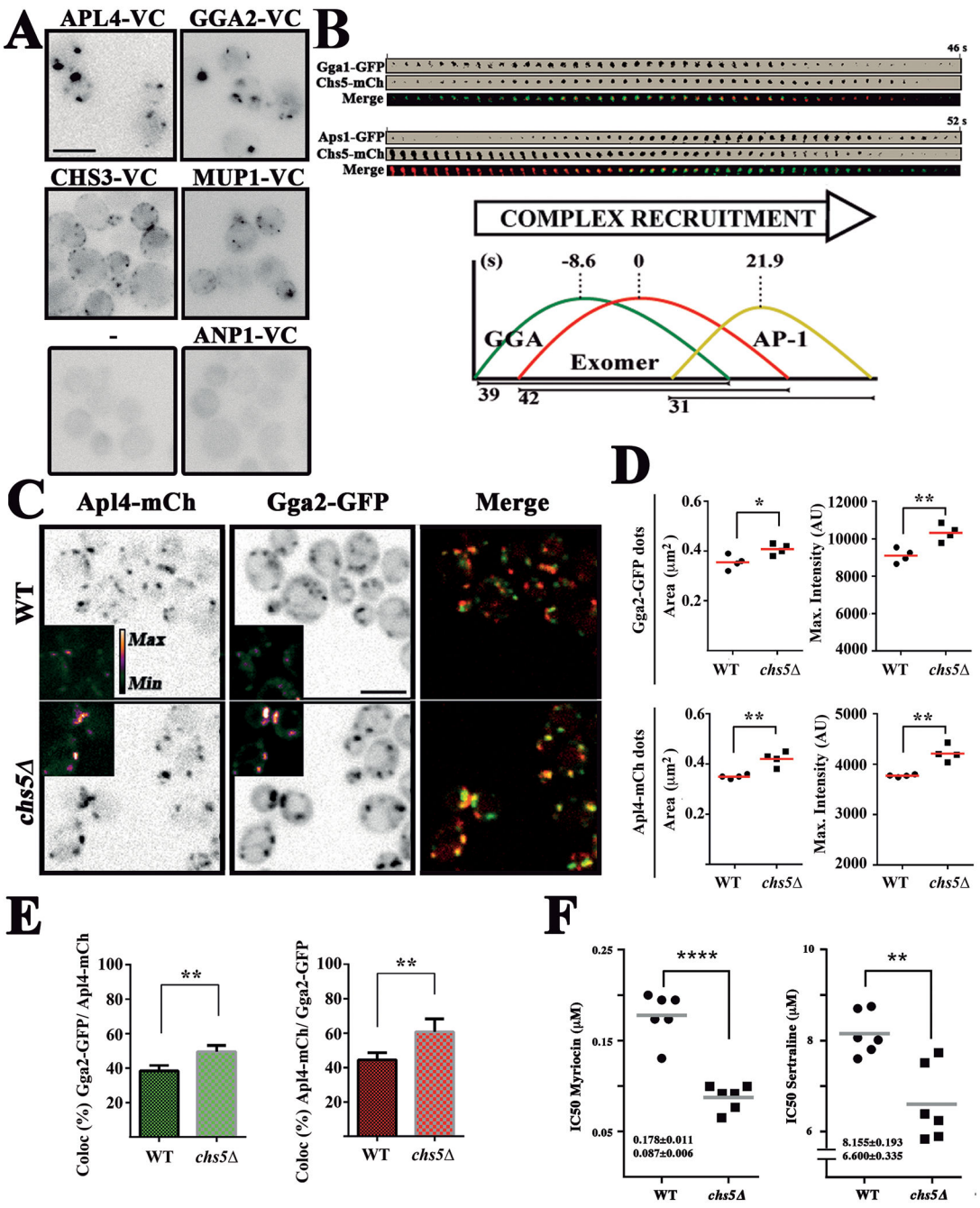


**Figure 4.**

Exomer contributes to TGN clathrin adaptor recruitment. (A) BIFC analysis of the interaction of Chs5-VN with the indicated proteins tagged with the VC fragment. Note the unexpected localization of Chs5-VN/Chs3-VC along the PM. (B) Time-lapse analysis of the recruitment of the clathrin adaptor complexes and exomer. Individual dots for each protein were visualized by two color confocal spinning disk microscopy over time. Graphs represent the average recruitment duration of each complex using exomer as a reference. For more detailed information see Figure S5. (C) Localization of Apl4-mCh and Gga2-GFP in

the wild-type and *chs5Δ* strains. Note the larger and more intense dots of both proteins in *chs5Δ* and the apparent increase in co-localization. (D) Quantitative analysis of Gga2-GFP and Apl4-mCh dots in the experiment shown in C. Note the significant increase in the area and intensity of the dots for both proteins in the absence of exomer. The results are the average of 4 independent experiments. (E) Co-localization analysis between Gga2-GFP and Apl4-mCh. The values are the average of four independent experiments. (F) Sensitivity of the indicated strains to myriocin and sertraline represented by the IC50 coefficient, calculated as described in the Material and Method section. Values represent the average of six independent experiments.

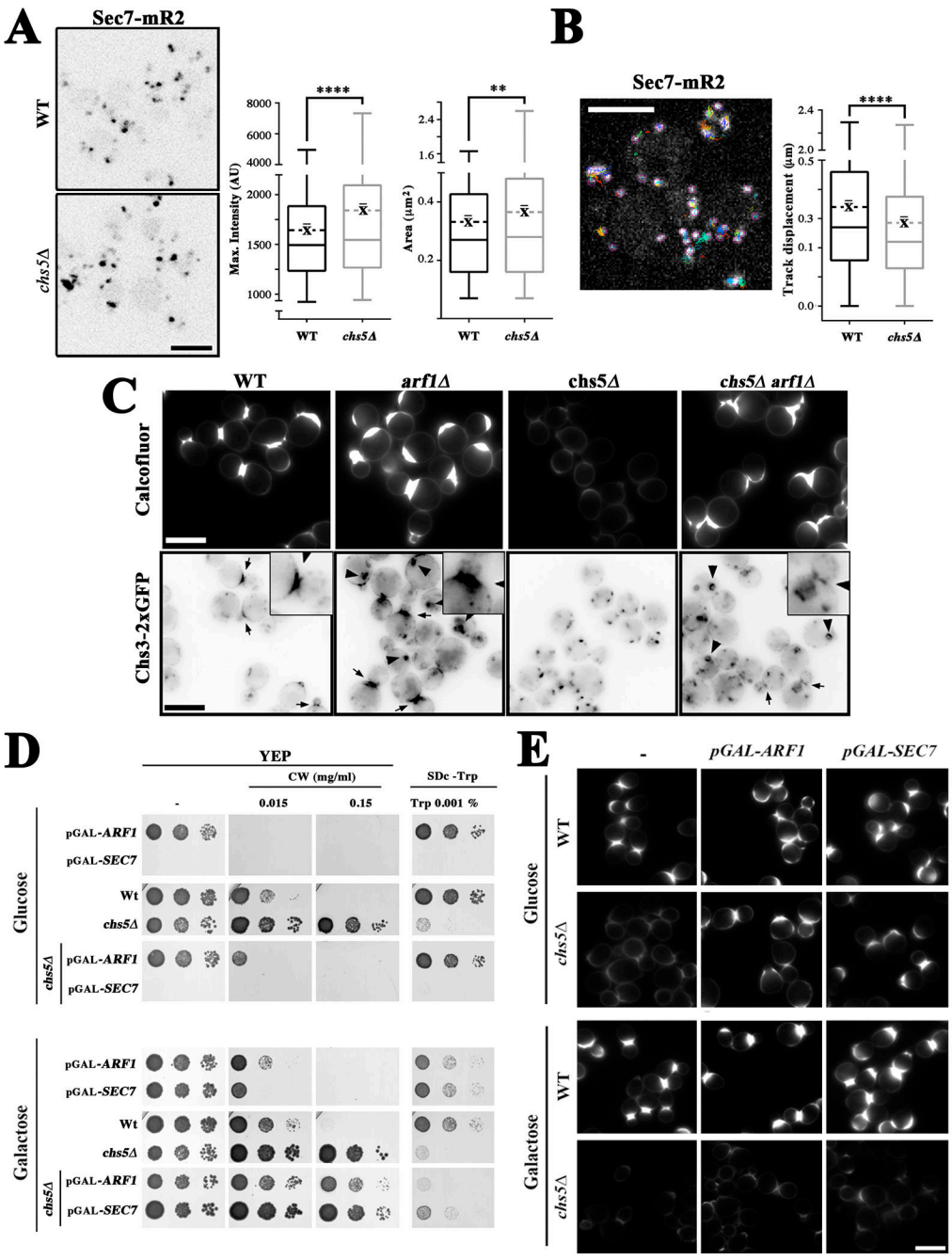


**Figure 5.**

Functional link between Arf1 GTPase and the exomer complex. (A) Localization of Sec7-mR2 in the wild-type and *chs5Δ* strains. The right panels show the quantitative analysis of Sec7-mR2 TGN structures using Macro2. The box-plots represent the intensity and the area of Sec7-mR2 dots (the average is represented by the dashed line, n ≥ 700 dots acquired in 4 independent experiments). (B) Analysis of Sec7-mR2 dynamics in the absence of exomer with the *TrackMate* ImageJ plugin. The Box-plots represent the average track displacement of Sec7-mR2 dots calculated from more than 2500 trajectories for each strain acquired

in 4 independent experiments (the average is represented by the dashed line). See Figure S6C for additional data on the dynamics of Sec7. (C) Effect of Arf1 deletion on chitin synthesis. Upper panels show calcofluor staining in the indicated strains. Lower panels show the localization of Chs3–2xGFP in the indicated strains. Arrows show the accumulation of Chs3 at bud necks and the arrowheads mark aberrant TGN/EE structures. (D) Effects of the deregulation of Arf1/Sec7 expression in cells expressing the indicated chromosomal genes from the GAL1 promoter in the wild-type or *chs5Δ* strains. Cells were grown O/N in YEP 2 % raffinose and 0.1 % galactose, serially diluted and spotted on the indicated media containing glucose (upper panel) or galactose (lower panel) as the carbon source. Growth was recorded after 2–3 days at 28ºC. Note how the pGAL1-*SEC7* strains were unable to grow on media containing glucose. (E) Calcofluor staining of multiple strains in which the indicated chromosomal gene is under the control of the GAL1 promoter. Cells were grown O/N as indicated above and transferred to the indicated media for two hours; then, calcofluor was added and chitin staining was visualized after an additional 90 minutes. Note that repression of *ARF1* and *SEC7* in glucose media restored calcofluor staining in the *chs5Δ* mutant.

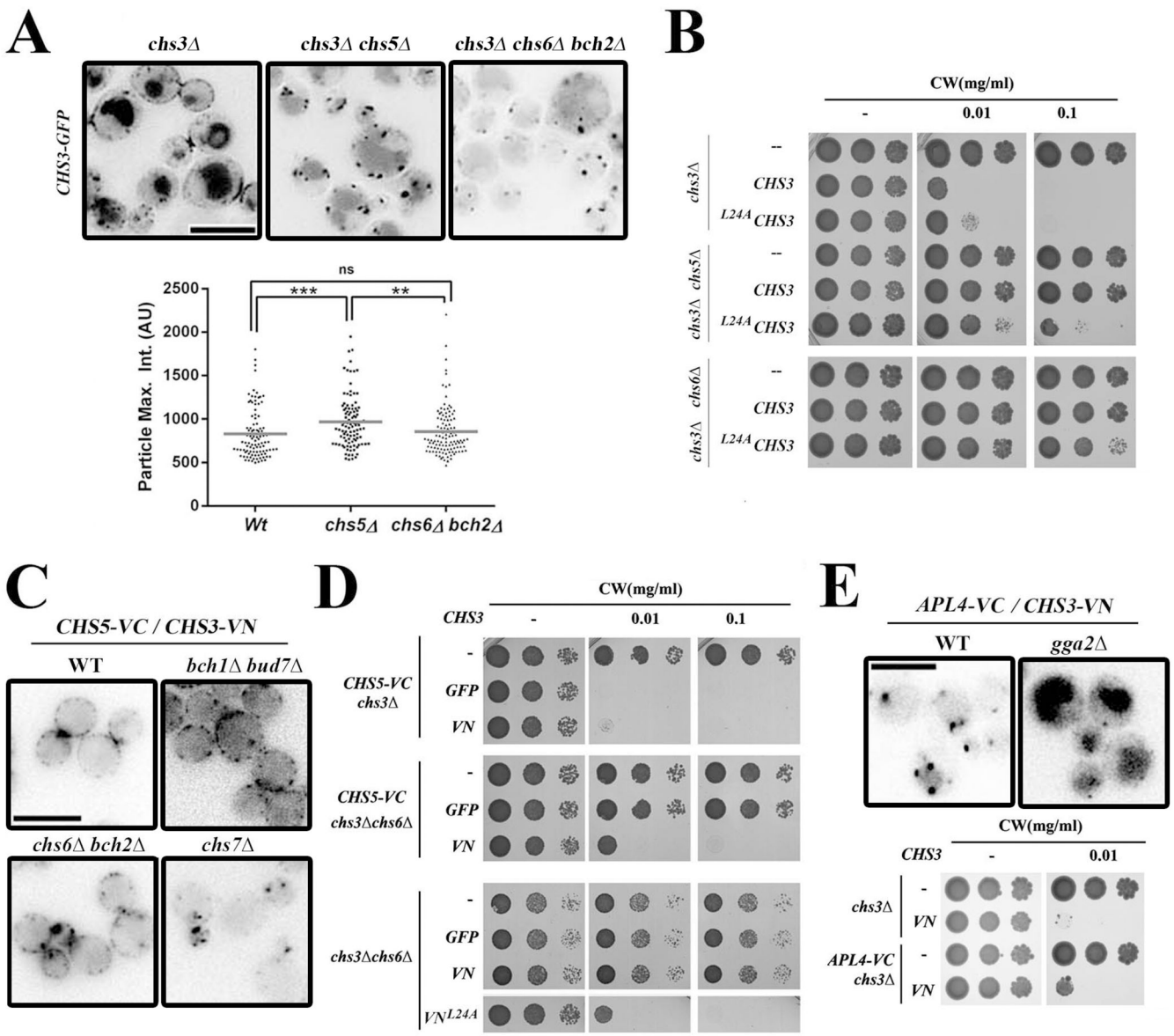


**Figure 6.**

Analysis of Chs3 transport reveals different phenotypes among the mutants of different exomer subunits and shows cargo competition between the exomer and AP-1 complexes. (A) Localization of Chs3-GFP in *chs5Δ* and *chs6Δ bch2Δ* mutants. Static images and quantitative analysis of the intracellular dots of Chs3 in both mutants are shown. Note the reduced diameter and intensity of Chs3-GFP in the *chs6Δ bch2Δ* strain compared to *chs5Δ*. (B) Calcofluor sensitivity of cells expressing wild-type Chs3 and mutant $^{L24A}$Chs3 proteins. (C) Analysis of the Chs3/Chs5 interaction by BIFC. Most of the signal is distributed along the PM, even in the absence of a functional exomer as in the *bud7Δ bch1Δ* double mutant. However, this localization is prevented if Chs3 exit from the ER is blocked as in the *chs7Δ* mutant. (D) Calcofluor resistance of the different Chs3 constructs in the indicated strains. Note that the interaction Chs5-VC/Chs3-VN suppressed the resistance of the *chs6Δ* mutant

to calcofluor, similar to the effects observed for the $^{L24A}$Chs3 protein. (E) Analysis of the Chs3/Apl4 interaction by BIFC. Upper panel shows localization of Chs3/Apl4 interaction. Lower panel shows calcofluor resistance of the indicated strains. Note that Apl4-VC/Chs3-VN interaction confers moderate resistance to calcofluor on its own (lower panel).

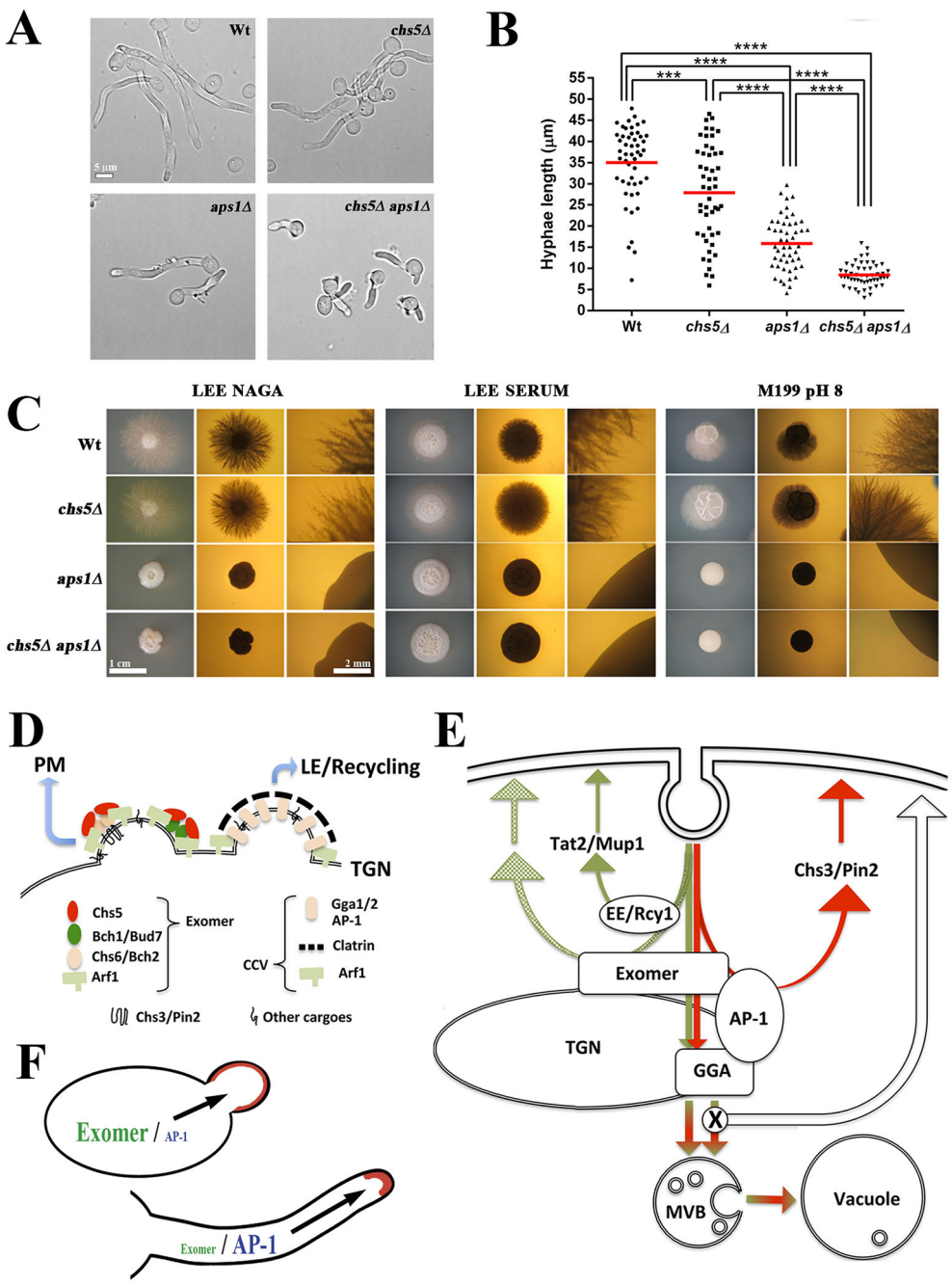


**Figure 7.**

Exomer and clathrin adaptors in protein sorting: implications of exomer and AP-1 relationship in *Candida albicans* physiology and a model for TGN sorting. (A) *C. albicans* cells of the indicated strains were induced for filamentation at 37ºC in filamentation media (YEPD, 80 mg/L uridine and 10 % fetal bovine serum). Images were acquired after 2 hours of growth. (B) Quantification of the length of the hyphae in the experiment shown in A. (C) *C. albicans* filamentation in different solid media. Individual cells were plated onto the indicated filamentation media and incubated for 3–4 days at 37ºC. Images were

acquired with a stereomicroscope with upper (left panel) or lower (central and right panels) illumination. Right panels present images with a higher amplification to show the details of filamentation (scales 1cm and 2mm). Note the absence of hyphae in the *aps1Δ* and *aps1Δ chs5Δ* mutants under all conditions tested. All tested strains are diploids and homozygous for the indicated genes. (D) Exomer and CCV are assembled at nearby localizations of the TGN and share a requirement for Arf1-GTPase activity. Exomer assembles as different complexes with different properties and facilitates the anterograde delivery of multiple proteins to the PM. CCV vesicles facilitate the late endosomal traffic of several proteins, affecting their recycling. (E) Exomer is required for the transport to the PM of a limited set of proteins that interact with both the exomer and AP-1 complexes (red lines). The anterograde traffic and the recycling of these *bona fide* exomer cargoes strictly depend on the coordinated action of both exomer and AP-1, a distinctive characteristic of *S. cerevisiae* cells. By contrast, exomer has a more general role in protein sorting at the TGN region that facilities polarized delivery of multiple proteins to the PM, independent of Rcy1-mediated recycling (green lines). In addition, exomer contributes to the correct assembly of the clathrin adaptor complexes, thereby, facilitating the proper late endosomal traffic of multiple proteins through the vacuole. Disruption of these clathrin adaptor complexes allows the transit of all these proteins to the PM by alternative pathways. PM: plasma membrane, TGN: trans-Golgi network; MVB: multi vesicular body. (F) A diagram showing the differential role of the exomer and AP-1 complexes in the polarized growth of fungi depending on how cells grow as yeasts or as hyphae.

**Table 1.**

Yeast strains used.

| Strain | Genotype | Origin / Reference |
|---|---|---|
| ***S. cerevisiae* strains** | | |
| CRM67 | W303, mat a, (*leu2-3,112 trp1-1 can1-100 ura3-1 ade2-1 his3-11,15*) | Lab. collection |
| CRM2268 | W303, mat a, *chs5Δ::natMx4* | Lab. Collection |
| CRM3066 | W303, mat a, *bch1 Δ::kanMx4 bud7Δ::natMx4* | (42) |
| CRM3081 | W303, mat a, *chs6Δ::kanMx4 bch2Δ::natMx4* | (42) |
| CRM3851 | W303, mat a, *tat2Δ::hphNT1* | This study |
| CRM3853 | W303, mat a, *chs5Δ::natMx4 tat2Δ::hphNT1* | This study |
| CRM3909 | W303, mat a, PGAL1-*TAT2::KanMx4* | This study |
| CRM3917 | W303, mat a, *chs5Δ::natMx4* PGAL1-*TAT2::KanMx4* | This study |
| CRM2868 | W303, mat a, PGAL1-GFP-*SSY1::KanMx4* | This study |
| CRM2871 | W303, mat a, *chs5Δ::natMx4* PGAL1-*GFP-SSY1 ::KanMx4* | This study |
| CRM3811 | W303, mat a, *STP1-3xHA::hphNT1* | This study |
| CRM3825 | W303, mat a, *STP1-3xHA::hphNT1 chs5Δ::natMx4* | This study |
| CRM3813 | W303, mat a, *GLN3-3xHa::hphNT1* | This study |
| CRM3827 | W303, mat a, *GLN3-3XHΔ::hphNT1 chs5Δ::natMx4* | This study |
| CRM3023 | W303, mat a, *GTR1-GFP::hphNT1* | This study |
| CRM3032 | W303, mat a, *chs5Δ::natMx4 GTR1-GFP::hphNT1* | This study |
| CRM3017 | W303, mat a, *TCO89-GFP::hphNT1* | This study |
| CRM3020 | W303, mat a, *chs5Δ::natMx4 TCO89-GFP::hphNT1* | This study |
| CRM2972 | W303, mat a, *GAP1-GFP::hphNT1* | This study |
| CRM2979 | W303, mat a, *chs5Δ::natMx4 GAP1-GFP::hphNT1* | This study |
| CRM2894 | W303, mat a, *TAT2-GFP::hphNT1* | This study |
| CRM2903 | W303, mat a, *chs5Δ::natMx4 TAT2-GFP::hphNT1* | This study |
| CRM3531 | W303, mat a, *MUP1-GFP::KanMx4* | This study |
| CRM3540 | W303, mat a, *MUP1-GFP::KanMx4 chs5Δ::natMx4* | This study |
| CRM3882 | W303, mat a, $TAT2^{52\text{-}53}$-*3xHA* (internal by *Delitto Perfetto*) | This study |
| CRM3890 | W303, mat a, $TAT2^{52\text{-}53}$-*3xHA chs5Δ:: kanMx4* | This study |
| CRM3862 | W303, mat a, *bul1Δ:: kanMx4* | This study |
| CRM3903 | W303, mat a, *bul2Δ:: hphNT1* | This study |
| CRM3880 | W303, mat a, *bul1Δ:: kanMx4 bul2Δ:: hphNTl* | This study |
| CRM3864 | W303, mat a, *chs5Δ:: kanMx4 bul1Δ:: kanMx4* | This study |
| CRM3950 | W303 mat a, *gga2Δ:: hphNT1 chs5Δ::kanMx4* | This study |
| CRM3526 | W303 mat a, *rcy1Δ:: kanMx4 gga1A:: natMx4* | Lab. Collection |
| CRM3602 | W303 mat a, *rcy1Δ:: kanMx4 gga2Δ:: hphNT1* | Lab. Collection |
| CRM4025 | W303 mat a, *rcy1Δ:: kanMx4 aps1Δ:: hphNT1* | This study |
| CRM3432 | W303 mat a, *APL4-VC::kanMx4 CHS5-VN::HIS3* | This study |
| CRM3477 | W303 mat a, *CHS5-VC::kanMx4* | This study |
| CRM3997 | W303 mat a, *CHS5-VN::kanMx4* | This study |
| CRM4003 | W303 mat a, *CHS5-VN::kanMx4 MUP1-VC::HIS3* | This study |

| Strain | Genotype | Origin / Reference |
|---|---|---|
| CRM4070 | W303 mat a, *CHS5-VN::kanMx4 GGA2-VC::HIS3* | This study |
| CRM2879 | W303 mat a, *SEC7-mRuby2::kanMx4* | This study |
| CRM2882 | W303 mat a, *chs5Δ::natMx4 SEC7-mRuby2::kanMx4* | This study |
| CRM4088 | W303 mat a, *arf1Δ::kanMx4* | This study |
| CRM4090 | W303 mat a, *chs5Δ::natMx4 arf1Δ::kanMx4* | This study |
| CRM1278 | W303 mat a, *chs3A:: URA3 chs5Δ:: natMx4* | Lab. Collection |
| CRM1590 | W303 mat a, *chs3A:: natMx4* | Lab. Collection |
| CRM3089 | W303, mat a, *bch1Δ::kanMx4 bud7Δ:: natMx4 chs3Δ::hphNT1* | This study |
| CRM3091 | W303 mat a, *chs6Δ::kanMx4 bch2Δ:: natMx4 chs3Δ::hphNT1* | This study |
| CRM4098 | W303 mat a, *chs3Δ:: URA3 chs6Δ::kanMx4* | This study |
| CRM3534 | W303 mat a, *CHS5-VC::kanMx4 gga2Δ:: hphNT1* | This study |
| CRM3511 | W303 mat a, *CHS5-VC::kanMx4 chs6Δ:: natMx4 bch2A::hphNT1* | This study |
| CRM3668 | W303 mat a, *CHS5-VC::kanMx4 bch1Δ:: hphNT1 bud7A:: natMx4* | This study |
| CRM3641 | W303 mat a, *CHS5-VC::kanMx4 chs7Δ:: hphNT1* | This study |
| CRM3674 | W303 mat a, *CHS5-VC::kanMx4 chs3Δ:: URA3* | This study |
| CRM3511 | W303 mat a, *CHS5-VC::kanMx4 chs6Δ:: natMx4* | This study |
| CRM3676 | W303 mat a, *CHS5-VC::kanMx4 chs6Δ:: natMx4 chs3Δ:: URA3* | This study |
| CRM3432 | W303 mat a, *APL4-VC::kanMx4* | This study |
| CRM3453 | W303 mat a, *APL4-VC::kanMx4 gga2Δ:: hphNT1* | This study |
| CRM3436 | W303 mat a, *chs3Δ::URA3 APL4-VC::kanMx4* | This study |
| CRM2248 | W303, mat a, *CHS5-mCherry::natMx4 APS1-GFP:: hphNT1* | Lab. Collection |
| CRM2533 | W303, mat a, *CHS5-mCherry::natMx4 GGA1-GFP:: hphNT1* | Lab. Collection |
| CRM808 | BY4741, mat a (*his3A1, leu2A0, met15A0, ura3A0*) | EUROSCARF |
| CRM1435 | BY4741, mat a, *chs3Δ::natMx4* | Lab. Collection |
| CRM2453 | BY4741, mat a, *chs3Δ::natMx4 chs5Δ::hphNT1* | Lab. Collection |
| CRM3922 | BY4741, mat a, *chs5Δ::natMx4* | Lab. Collection |
| CRM3924 | BY4741, mat a, *art1Δ::kanMx4chs5Δ::natMx4* | This study |
| CRM3926 | BY4741, mat a, *art2Δ::kanMx4chs5Δ::natMx4* | This study |
| CRM3928 | BY4741, mat a, *art3Δ::kanMx4chs5Δ::natMx4* | This study |
| CRM3930 | BY4741, mat a, *art4Δ::kanMx4chs5Δ::natMx4* | This study |
| CRM3932 | BY4741, mat a, *art5Δ::kanMx4chs5Δ::natMx4* | This study |
| CRM3934 | BY4741, mat a, *art6Δ::kanMx4chs5Δ::natMx4* | This study |
| CRM3935 | BY4741, mat a, *art7Δ::kanMx4chs5Δ::natMx4* | This study |
| CRM3937 | BY4741, mat a, *art8Δ::kanMx4chs5Δ::natMx4* | This study |
| CRM3939 | BY4741, mat a, *art9Δ::kanMx4chs5Δ::natMx4* | This study |
| CRM3941 | BY4741, mat a, *art10Δ::kanMx4 chs5Δ::natMx4* | This study |
| CRM4019 | BY4741, mat a, *GGA2-GFP::hphNT1 APL4-mCherry:: natMx4* | This study |
| CRM2761 | X2180-1A, mat a (*SUC2 mal mel gal2 CUP1*) | Francisco del Rey |
| CRM2763 | X2180-1A, mat a, *chs5Δ::kanMx4* | This study |
| CRM3957 | X2180-1A, mat a, *tat2Δ::kanMx4* | This study |
| CRM3959 | X2180-1A, mat a, *chs5Δ::kanMx4 tat2Δ::kanMx4* | This study |
| CRM2783 | X2180-1A, mat a, *ssy1Δ::natMx4* | This study |

| Strain | Genotype | Origin / Reference |
|---|---|---|
| CRM3010 | X2180-1A, mat a, *ssy1Δ::natMx4 chs5Δ::kanMx4* | This study |
| CRM4311 | W303, mat a, *ARF1-GFP: :hphNT1* | This study |
| CRM4134 | W303, mat a, *CHS3-2xGFP::hphNT1* | This study |
| CRM4136 | W303, mat a, *CHS3-2xGFP::hphNT1 chs5Δ::natMx4* | This study |
| CRM4140 | W303, mat a, *CHS3-2xGFP::hphNT1 arf1Δ::kanMx4* | This study |
| CRM4138 | W303, mat a, *CHS3-2xGFP::hphNT1 chs5Δ::natMx4 arf1Δ::kanMx4* | This study |
| CRM4157 | W303, mat a, PGAL1-*ARF1::KanMx4* | This study |
| CRM4159 | W303, mat a, *chs5Δ::natMx4 PGAL1-ARF1::KanMx4* | This study |
| CRM4302 | W303, mat a, *PGAL1-SEC7::KanMx4* | This study |
| CRM4339 | W303, mat a, *PGAL1-SEC7::KanMx4 chs5Δ::natMx4* | This study |
| CRM2818 | BY4741, mat a, *CHS5-GFP::hphNT1* | Lab. Collection |
| CRM4160 | BY4741, mat a, *CHS5-GFP::hphNT1 arf1Δ::kanMx4* | This study |
| CRM4594 | W303, mat a, *CHS5-VN::kanMx4 ANP1-VC::HIS3* | This study |
| CRM4586 | W303, mat a, *CHS5-mCherry::natMx4 GGA1-GFP::hphNT1 arf1Δ:: kanMx4* | This study |
| CRM4584 | W303, mat a, *CHS5-GFP::hphNT1* | This study |
| CRM4573 | W303, mat a, *PGAL1-GGA2::KanMx4 CHS5-GFP::hphNT1* | This study |
| CRM4118 | W303, mat a, *APS1-GFP::hphNT1* | This study |
| CRM4153 | W303, mat a, *PGAL1-GGA2::KanMx4 APS1-GFP::hphNT1* | This study |
| CRM4571 | W303, mat a, *PGAL1-BUD7::KanMx4 APS1-GFP::hphNT1* | This study |
| CRM4576 | W303, mat a, *PGAL1-BCH1::KanMx4 APS1-GFP::hphNT1* | This study |
| ***C. albicans* strains** | | |
| CRM2499 | BWP17, (*ura3::imm434/ura3::imm434 his1 ::hisG/his1::hisG arg4: :hisG/ arg4::hisG*) | (75) |
| CRM2531 | BWP17, *Cachs5Δ::ARG4/Cachs5Δ::HIS1* | Lab. Collection |
| CRM3258 | BWP17, *Caaps1Δ::SAT1/Caaps1 Δ::URA3* | This study |
| CRM3261 | BWP17, *Cachs5Δ::ARG4/Cachs5Δ::HIS1 Caaps1Δ::SAT1/Caaps1Δ::URA3* | This study |

**Table 2.**

Plasmids used.

| Plasmid | Genotype | Origin / Reference |
|---|---|---|
| CRM160 | pRS313 (*HIS3*) | Lab collection |
| CRM161 | pRS314 (*TRP1*) | Lab collection |
| CRM264 | pRS315 (*LEU2*) | Lab collection |
| CRM265 | pRS316 (*URA3*) | Lab collection |
| CRM166 | pRS426 (*URA3*) | Lab collection |
| CRM2546 | pAG25 (*natMx4*) | (32) |
| CRM1188 | pUG6 (*kanMx4*) | (32) |
| CRM2546 | pUG72 (*URA3*) | (32) |
| CRM1451 | pFA6a-*hphNT1* | (32) |
| CRM1807 | pFA6a-*3xHΔ::hphNT1* | (34) |
| CRM1995 | pFA6a-*GFP::hphNT1* | (34) |
| CRM1811 | pFA6a-*GFP::natMx4* | (34) |
| CRM2653 | pFN21 (*mCherry::natMx4*) | (34) |
| CRM2037 | pFA6a-*kanMX4*-pGAL1 | (33) |
| CRM2827 | pFA6a-*kanMX4*-pGAL1-GFP | (33) |
| CRM2360 | pGSHU (CORE Delitto Perfetto) | (35) |
| CRM3469 | pFA6a-***V****enus****C****terminal::HIS3* | (39) |
| CRM3470 | pFA6a-***V****enus****N****terminal::HIS3* | (39) |
| CRM3471 | pFA6a-***V****enus****C****terminal:: kanMX4* | (39) |
| CRM3472 | pFA6a-***V****enus****N****terminal:: kanMX4* | (39) |
| CRM2328 | pFA6a- link-*yomRuby2::CaURA3* | (76) |
| CRM1131 | pRS315::*CHS3-GFP* | (77) |
| CRM3456 | pRS315::*CHS3-VN::HIS3* | This study |
| CRM2084 | pRS315::$CHS3^{L24A}$-*GFP* | (78) |
| CRM1868 | pRS315-GFP-Snc1 | Anne Spang |
| CRM3236 | pFA-*CaHIS1* | (79) |
| CRM3238 | pFA-*CaARG4* | (79) |
| CRM3240 | pFA-*CaURA3* | (79) |
| CRM2583 | pFA-*GFP-SAT1* | (80) |

**Table 3.**

ImageJ Macros used:

**Macrol: Pre-filtering for dot co-localization**

```
showMessage("Open Channel Red"); //Select Channel Red
open();
red = getTitle();
showMessage("Open Channel GFP"); //Select Channel GFP
open();
gfp = getTitle(); //Then, we are going to filter both channels
selectWindow(gfp);
run("Median…", "radius=1 stack"); //Filtering
run("Unsharp Mask…", "radius=2 mask=0.5 stack"); //Filtering
selectWindow(red);
run("Median…", "radius=1 stack"); //Filtering
run("Unsharp Mask…", "radius=2 mask=0.5 stack"); //Filtering
run("JACoP "); //Open JACoP plugin
```

**Macro2: Analyze dots**

```
showMessage("Open the Image"); //Select image
open();
run("Duplicate…", " "); //We want to do the segmentation in a copy of the original, therefore we duplicate
run("Median…", "radius=1"); //Filtering
run("Unsharp Mask…", "radius=2 mask=0.50"); //Filtering
run("Threshold…"); // to open the threshold window if not opened yet
waitForUser("Set the threshold and press OK, or cancel to exit macro"); // pauses the execution and lets you access ImageJ manually
run("Analyze Particles…"); //to take the ROIs
waitForUser("Finally, use these ROIs in the original window"); //A note to correctly continue after the macro
```

**Macro3: Counting colonies**

```
showMessage("Open the Image"); //Select image with colonies
open();
rename("Initial");
run("Duplicate…", " ");
run("Threshold…"); // to open the threshold window if not opened yet
waitForUser("set the threshold and press OK, or cancel to exit macro"); // pauses the execution and lets you access ImageJ manually as long as you dont' press OK, which resumes the macro execution
run("Convert to Mask"); // to binarize, if you use this command, dont' press 'Apply' in the threshold window
run("Watershed"); //to separate close colonies
rename("Mask");
waitForUser("Calibration: Draw a line along the Petri dish \nand introduce the known size in Analize/SetScale, then press OK");
run("Threshold…");
waitForUser("Set the threshold and press OK, or cancel to exit macro"); // pauses the execution and lets you access ImageJ manually
run("Analyze Particles…"); //to take the ROIs
```